UNIVERSIDAD NACIONAL DE COLOMBIA

Effect of cement and aggregate substitution in a conventional concrete with alkaline activated cement (AAC) and lightweight aggregates (LWA)

TRADUCCION AL ESPAÑOL:
Efecto de la sustitución de cemento y agregados en un concreto convencional por Cemento Activado Alcalinamente (CAA) y Agregados Livianos (AL)

DANIELA GONZÁLEZ BETANCUR

Universidad Nacional de Colombia
Faculty of Architecture, School of Construction
Medellin, Colombia
2023

Effect of cement and aggregate substitution in a conventional concrete with alkaline activated cement (AAC) and lightweight aggregates (LWA)

Daniela González Betancur

A thesis submitted to the Faculty of Graduate Studies and Research in partial fulfillment of the requirements for the degree of:
Master of Science in Construction

Advisors:
Ph.D. Ary Alain Hoyos Montilla
Ph.D. Jorge I. Tobón

Research line:
New Alternative Concrete Materials
Researh Group:
Cement and Construction Materials (CEMATCO)

Universidad Nacional de Colombia
Faculty of Architecture, School of Construction
Medellín, Colombia
2023

"There is no such thing as distance when you have a motive"

Jane Austen

Declaration

I take the liberty of stating that I have carried out the present thesis autonomously and with the sole aid of the means permitted and not different from those mentioned in the thesis itself. All passages that have been taken verbatim or figuratively from published and unpublished texts, I have acknowledged in the present work. No part of this work has been used in any other type of thesis.

Medellín, Antioquia, 02.08.2023

Daniela González Betancur
1.152.695.357

Acknowledgments

I am deeply grateful to my advisors, Professor Ary Alain Montilla and Jorge Iván Tobón, for their invaluable guidance and support. I am so grateful for their insights, advice, and encouragement. I am truly fortunate to have had them as my mentors. I would also like to thank my colleagues in the CEMATCO research group for their valuable feedback and suggestions. Their insights have helped me to improve my research and to make my thesis stronger. I have learned so much from working with them, and I am grateful for their friendship and collaboration. In addition, I would like to thank the faculty of Architecture for providing me with financial support throughout my master studies. This funding has allowed me to focus on my research and attend conferences and workshops.

Also, I would like to thank my family and friends for their love and support. They have been there for me through thick and thin, and I am so grateful for their encouragement. I am truly grateful for all of the help and support that I have received during my master journey. It has been an amazing experience, and I am excited to see what the future holds.

Finally, I would like to express my sincere gratitude to myself for believing in myself, for working hard, for never giving up, and for never taking a day off. I know that I have accomplished a lot, and I am proud of what I have achieved. I am also grateful for the opportunity to have learned and grown so much during this journey.

Abstract

According to Global Cement and Concrete Association (GCCA), in 2020, the worldwide production of concrete is 14^{13} m^3/year. This massive utilization of concrete production has a significant environmental impact due to the extraction of its raw materials and the production of Ordinary Portland Cement (OPC). On the other hand, polymers are used in almost all areas of our daily lives. it is estimated that by the year 2050, their production could reach 33 billons t/year. In particular, Expanded Polystyrene (EPS) is used as thermal insulation in 85 % of cases, generating a high volume of this plastic waste. Thus, alternative materials such as blended cement and recycled EPS Lightweight Aggregate (EPS LWA) can reduce this detrimental environmental impact. The objective of this research project is to determine the effect on Interfacial Transition Zone (ITZ) porosity and compressive strength of a Lightweight Aggregate Concrete (LWAC) produced with a blended cementitious matrix composed of OPC and Alkaline Activated Cement (AAC) based on Fly Ash (FA) and an additional source of Calcium (Lime). An experimental design was carried out to identify the proportion of alternative cementitious material and EPS LWA that would provide the highest compressive strength. For this purpose, a compressive strength test was performed at 7^{th} and 28^{th} days of curing. Having the proportions of the alternative materials, a complementary sample was made to evaluate mechanical performance and perform a quantitative analysis of the porosity of the ITZ. Finally, the compressive strength and porosity of ITZ were correlated to evaluate the influence of ITZ microstructure on the mechanical properties of LWAC. X-Ray Diffraction (XRD) and Fourier Transform Infrared Spectroscopy (FTIR) were used to identify the formation of gels due to alkaline activation. From this project, it was concluded that the generation of hydration products such as Calcium Aluminate Silicate Hydrate (C-A-S-H), caused the densification of the ITZ. However, the reduction in compressive strength observed in the LWAC manufactured in this project could be explained by the anhydrous phases seen in Backscatering Scanning Electron Microscopy (BSEM) images and lower raw material dissolution observed in XRD. Incorporating EPS LWA and Expanded Clays (EC) in an LWAC also physically impacts compressive strength by redistributing stresses in the microstructure of the LWAC. This is due to the inclusion of brittle and ultra-soft materials that differ from cement paste. Furthermore, the hydrophobicity of EPS LWA causes a lack of adherence of the cementitious material to this LWA. As a result, compression fracture of the material will occur around the EPS LWA in the void space between the cementitious material and the EPS LWA. Despite that, the compressive strength of the LWAC obtained in this research project could be used to design a concrete structure according to Colombian technical standards for structural design (NSR-10). Thus decreasing the dead loads directly related to its own weight. The results also indicated that it is possible to substitute up to 70 % of the OPC with alternative cementitious materials. This could ultimately translate into savings in the total cost of the work and, with the use of FA and Lime, a reduction in CO_2. emissions.

Keywords: Interfacial Transition Zone, Compressive Strength, Lightweight Concrete, Alkali-Activated cement, Lightweight Aggregate.

Resumen

Según la Asociación Mundial del Cemento y el Concreto (GCCA), en 2020, la producción mundial de concreto será de 14^{13} m^3/año. Esta utilización masiva de la producción de concreto tiene un impacto medioambiental significativo debido a la extracción de sus materias primas y a la producción de Cemento Portland Ordinario (OPC). Por otro lado, los polímeros se utilizan en casi todos los ámbitos de nuestra vida cotidiana. Se calcula que para el año 2050 su producción podría alcanzar las 33 billones t/año. En particular, el Poliestireno Expandido (EPS) se utiliza como aislante térmico en el 85 % de los casos, generando un elevado volumen de este residuo plástico. Por lo tanto, los materiales alternativos como el cemento hibrido y el árido ligero de EPS reciclado (EPS LWA) pueden reducir este impacto medioambiental perjudicial. El objetivo de este proyecto de investigación es determinar el efecto sobre la porosidad de la Zona de Transición Interfacial (ITZ) y la resistencia a la compresión de un Concreto con Áridos Livianos (LWAC) producido con una matriz cementante mezclada compuesta de OPC y Cemento Alcalino Activado (AAC) basado en Cenizas Volantes (FA) y una fuente adicional de Calcio (Cal). Se llevó a cabo un diseño experimental para identificar la proporción de material cementante alternativo y EPS LWA que proporcionaría la mayor resistencia a la compresión. Para ello, se realizó un ensayo de resistencia a la compresión a los 7 y 28 días de curado. Disponiendo de las proporciones de los materiales alternativos, se realizó una muestra complementaria para evaluar el comportamiento mecánico y realizar un análisis cuantitativo de la porosidad de la ITZ. Por último, se correlacionaron la resistencia a la compresión y la porosidad del ITZ para evaluar la influencia de la microestructura del ITZ en las propiedades mecánicas del LWAC. La difracción de rayos X (XRD) y la espectroscopia infrarroja por transformada de Fourier (FTIR) se utilizaron para identificar la formación de geles debido a la activación alcalina. A partir de este proyecto, se concluyó que la generación de productos de hidratación, como el silicoaluminato de calcio hidratado (C−A−S−H), causó la densificación de la ITZ. Sin embargo, la reducción de la resistencia a la compresión observada en el LWAC fabricado en este proyecto podría explicarse por las fases anhidras observadas en las imágenes de Microscopía Electrónica de Barrido por Retrodispersión (BSEM) y la menor disolución de materia prima observada en el XRD. La incorporación de EPS LWA y arcillas expandidas (EC) en un LWAC también afecta físicamente a la resistencia a la compresión al redistribuir las tensiones en la microestructura del LWAC. Esto se debe a la inclusión de materiales quebradizos y ultrablandos que difieren de la pasta de cemento. Además, la hidrofobicidad del EPS LWA provoca una falta de adherencia del material cementante a este LWA. Como resultado, la fractura por compresión del material se producirá alrededor del EPS LWA en el espacio vacío entre el material cementante y el EPS LWA. A pesar de esto, la resistencia a la compresión del LWAC obtenida en este proyecto de investigación podría ser utilizada para diseñar una estructura de concreto de acuerdo con las normas técnicas colombianas para el diseño estructural (NSR-10). Disminuyendo así las cargas muertas directamente relacionadas con su propio peso. Los resultados también indicaron que es posible sustituir hasta 70 % del OPC con materiales cementantes alternativos. Esto podría traducirse finalmente en un ahorro en el coste total de la obra y, con el uso de FA y Cal, en una reducción de las emisiones de CO_2.

Keywords: Zona de Transición Interfacial, Resistencia a Compresión, Concreto Aligerado, Cemento Activado Alcalinamente, Árido Liviano.

Production Associated to this Research

Congress Participation

- D. González-Betancur, Hoyos-Montilla A., J. I. Tobón. August 29^{th} to September 3^{rd}, 2021. Effect of artificial lightweight aggregates on Interfacial Transition Zone in concrete. Oral presentation at *75th RILEM Annual Week and International Conference On Advances In Sustainable Construction Materials And Structures.*

- Pérez J. J., Taborda I., D. González-Betancur, Restrepo A., Zapata N., Restrepo O. J. December 10^{th}, 2021.Lightweight concrete manufacture from hybrid cement, OPC-AAC, and thermoplastic wastes for applying a thermal behavior design. *1^{st} Research Seminar on Mineral Resources, Materials and Nanotechnology (1^{st} SIRMMN).*

- Pérez J. J., Taborda I., D. González-Betancur, Restrepo A., Zapata N., Restrepo O. J. May 11^{th} to 13^{th} 2022. Physico-mechanical evaluation and thermal performance of lightweight concretes made from OPC-AAC hybrid cements and thermoplastic wastes (HERMES 54093). *XXI Encuentro Internacional de Semilleros de Investigación RedCOLSI 2023.*

- D. González-Betancur, Hoyos-Montilla A., J. I. Tobón, N. Betancur-Granados. July 24^{th} to 28^{th} 2022. Study on interfacial transition zone propierties of lightweight aggregates in concrete. Poster presentation at *Pan American Ceramics Congress and Ferroelectrics Meeting of Americas (PACC-FMAs).*

- D. González-Betancur, Hoyos-Montilla A., J. I. Tobón. October 26^{th} to 28^{th}, 2022. Blended cement and its effect on compressive strength in lightweight concrete. Oral presentation at *XI International Congress of Materials (XI CIM 2022).*

Publications

- D. González-Betancur, Hoyos-Montilla A., J. I. Tobón. 2023. *Effect of artificial lightweight aggregates on Interfacial Transition Zone in Concrete.* Book Chapter ISSN: 22110844. RILEM Books Series. DOI: 10.1007/978-3-031-21735-7_54.

Projects

- *Lightweight concrete Manufacture from OPC-AAC hybrid cements and thermoplastic wastes, for the application of thermal performance design* (HERMES Code: 54093). September to March, 2021. Call For Research, Creation, Or Innovation Seedbeds At The National University Of Colombia, Medellin Campus-2021: Projects For Introduction To Research, Creation, Or Innovation.

- *Effect of cement and aggregate substitution in a conventional concrete with alkaline activated cement (AAC) and lightweight aggregates (LWA)* (HERMES Code: 53925). March 2022-2023. Call For Young Researchers And Innovators In The Framework Of The Economic Reactivation 2021: Mechanism 1, Linking Of Young Undergraduate Researchers And Professionals In R&D+I Projects.

- *Strengthening The Scientific Capabilities Of The Universidad Nacional De Colombia, Campus Orinoquia Through The Project: Manufacture Of Environmentally Friendly Cement For Improving Pavements Of Tertiary Roads In The Llanos Region* (HERMES Code: 45939). August 2021-2024. 8^{th} Call of the Biennial Plan of the SGR CTeI Fund.

- *Proposal For Technical Support For Evaluating And Improving Hydraulic Cements Produced By Vallenato Cements* (HERMES Code: 35543). October 2022 to January 2023.

Research internship

- *École Polytechnique Fédérale de Lausanne*. LC^3 Doctoral School: Characterization Methods of Blended Cement. Laussane, Switzerland. February 6^{th} to 9^{th} 2023.

Scholarships

- Resolution M.DFAr-0206. April 15^{th} to July 15^{th}, 2021: Project Specialization In Building Pathology And Supervising Techniques - SIA 3545.

- Resolution M.DFAr-0635. August 31^{st}, 2021 to January 31^{th}, 2022: Project Operating Expenses Of The Research Management Unit - UGI Faculty Of Architecture.

- Resolution M.DFAr-0315. March 29^{th} to July 31^{th}, 2022: Project Specialization In Building Pathology And Supervising Techniques - SIA 3545.

Table of Contents

Figure List

Table List

Abbreviation List

Abbreviation	Terminology
AAC	Alkaline Activated Cement
AAFC	Alkaline Activated Fly Ash Concrete
AASC	Alkaline Activated Slag Concrete
AAFSC	alkali-activated fly ash-slag concrete
Al	Alumina
BSEM	Backscatering Scanning Electron Microscopy
Ca	Calcium
C-A-S-H	Calcium Aluminate Silicate Hydrate
CH	Calcium Hydroxide
C-S-H	Calcium silicate Hydrate
EC	Expanded Clays
ETM	Thermoplastic Microspheres
EPS	Expanded Polystyrene
FAC	Fly Ash Hollow Spheres
FA	Fly Ash
FTIR	Fourier Transform Infrared Spectroscopy
HGM	Glass microspheres
ITZ	Interfacial Transition Zone
LWAC	Lightweight Aggregate Concrete
LWA	Lightweight Aggregate
LWC	Lightweight Concrete
N-A-S-H	Sodium Aluminosilicate Hydrate
NTC	Colombian Technical Standard
NWC	Normal Weight Concrete
NWA	Conventional Aggregate
OPC	Ordinary Portland Cement
PET	Polyethylene Terephthalate
SEM	Scanning Electron Microscopy
SH	Sodium hydroxide
SS	Sodium silicate
TGA	Thermogravimetric Analysis

Abbreviation	**Terminology**
XRD	X-Ray Diffraction

1 Chapter 1: Preface

This thesis is presented in five chapters: preface, background, experimental program, analysis of results and conclusions. The first chapter is an introduction that presents the research problem, its relevance and the objectives of this master's thesis project. The second chapter presents and discusses the literature review carried out for the approach of this project. The third chapter presents the work methodology and the experimental program to achieve the proposed objectives. The fourth chapter presents the discussion and analysis of the results, starting with the characterization of the raw materials. Subsequently, the effect of the cementitious matrix and lightweight aggregates on two study variables, compressive strength and interfacial transition zone. Finally, the correlation between the two study variables is presented; the conclusions of this project are presented in chapter five, in addition to including some recommendations for future research.

Lightweight Aggregate concrete (LWAC) is not a modern achievement in materials technology. The first European references to this material date from two thousand years ago during the early Roman Empire. The Pantheon in Rome, Italy, was built in 128 B.C., and can be cited as one of the best-known examples. Unfortunately, after the collapse of the Roman Empire, the use of LWAC was limited due to the low availability and variability of natural lightweight aggregates, until the development and production of industrialized lightweight aggregates in the 19^{th} and 20^{th} centuries marked a historical turning point for concrete technology [1, 2, 3]. A LWAC refers to any concrete produced with a dry-state density less than 2000kg/m^3 [4]. In addition, it may consist entirely of lightweight aggregates (LWA) or a mix of LWA and conventional aggregates. LWACs are remarkably adaptable to seismic design, due to the significant reduction of inertial forces, in elements designed with this material [1]. Since it reduces the unit weight of the element and, consequently, the lateral forces acting on the structure during seismic events since inertial forces depend linearly on the mass of the structure [5].

On the other hand, related to its technical properties have prevented its widespread use in the building industry as a structural element [6]. The brittleness of lightweight concrete is higher than that of normal weight concrete (NWC) for the same mix ratio and compressive strength [7]. In addition, their mechanical properties are also lower than those of NWC [7, 8, 9]. For this reason, considerable efforts have been devoted to improving its properties through the study of its microstructure, particularly the mechanisms responsible for forming

the interfacial transition zone (ITZ) [10, 11, 12, 13], related, among other things, such as the absorption and release of water, which is a characteristic of LWA, due to their high porosity [2, 10]. The LWAs have higher water absorption and subsequent water release, increasing the degree of hydration of the paste around the aggregate and the amount of free water, causing the adjacent paste to develop a structure with higher porosity [2, 10]. Consequently, the use of a LWA with non-absorbent properties has been proposed [8, 14, 15, 16, 17, 18, 19].

On the other hand, a LWAC could be produced with any available cement, usually ordinary Portland cement (OPC) or supplementary cementitious materials (blast furnace slag, fly ash, silica fume, among others). Although it has already been demonstrated that LWAC with good performance could be made with ordinary Portland cement (OPC) [16], and an alkaline activated cement (AAC) [20] separately, the production of LWAC with blended cement has not been reported so far, which has great potential because this cement is the most expeditious way to achieve Portland cement substitution. This research project focuses on the effect on the ITZ microstructure and compressive strength of replacing cement and aggregates in conventional concrete with alkaline activated cement and lightweight aggregates.

1.1. Problem Statement

Concrete production seeks to reduce the exploitation of natural sources to extract raw materials by applying strategies that reduce its environmental impact. Therefore, the scientific community has focused on finding alternative materials that could partially or totally replace Portland cement and natural aggregates used in concrete production. On the other hand, polymers have many applications in different economic sectors and their manufacture has grown exponentially, with recycling being the most efficient way to treat polymeric waste. Several studies have shown that it is possible to reuse plastic waste in the construction industry and the use of recycled polymers as a substitute for stone aggregates in LWAC manufacturing has been explored.

The use of AAC has been shown to reduce the ITZ size of LWACs, increasing their density and increasing the compressive strength of the overall system. However, extensive use of this material is impractical due to the availability of precursors worldwide. Thus, a blended cement that blends OPC with an AAC could be a viable alternative, but its effect on ITZ is not yet clear.

1.1.1. Research Question

What is the effect of replacing cement and aggregates in conventional concrete with alkali-activated cement and lightweight aggregates on ITZ and compressive strength?

1.2. Research Significance

According to Global Cement and Concrete Association (GCCA), in 2020, globally concrete production is around 14^{13} m^3/year, and cement raw materials and concrete aggregates are the most extracted mineral resource in the world [21, 22]. The permanent extraction of these raw materials significantly adversely affects ecosystems and the communities around it [23, 24, 25]. Therefore, reducing the quantities of virgin aggregates extracted is essential if it want to preserve the natural ecosystems for future generations. On the other hand, polymers are used in almost all areas of our daily lives. They have many applications in different economic sectors, and their manufacture has grown exponentially, it is estimated that by the year 2050, their production could reach 33 billion t/year [26, 27, 28]. All types of plastic used in our daily lives eventually become waste; approximately 6.5 million t/year of polymeric waste are generated worldwide [26, 27, 28]. In particular, Expanded Polystyrene (EPS) is used as thermal insulation in 85 % of cases, generating a high volume of this plastic waste [29]. Recycling is the best solution for dealing with polymeric waste, with one of the most widely used methods being the reuse of plastic waste in the construction industry. Studies have shown that plastic could be used in concrete, and the use of recycled polymers as a replacement for stone aggregates has been explored [17, 30, 31]. Polymers could effectively reduce the density and brittleness of concrete or mortar. They have also demonstrated good performance in their thermal, permeability, and acoustic insulation properties [17, 18, 19, 30, 31, 32, 33].

In addition, ordinary Portland cement (OPC) results from calcination of $CaCO_3$, silicoaluminates minerals, and other complementary minerals at a 1450 °C. The production of 1 ton of OPC directly generates $0.5 - 0.60$ ton of CO_2; this process requires coal-based fuels, which produce 0.40 ton of CO_2; this productive sector is responsible for the release of 8 % of CO_2 emissions into the atmosphere [34, 35, 36, 37]. Given the high potential for pollution in the manufacture of OPC, it has been of great interest to replace OPC with alternative cementitious materials, among which AAC stands out. Thus, according to Davidovits [35], it is possible to achieve a $25\,\% - 30\,\%$ reduction in CO_2 emissions by combining OPC with replacement materials such as coal fly ash (FA). Weil et al.[38, Chapter10] conducted a life cycle study for these materials and concluded that the global warming potential of concrete using AAC, with FA as a precursor is approximately 70 % lower than that of concrete with OPC.

AAC is material with high industrial application, partly due to its technical and environmental advantages (low CO_2 emissions), the ease of implementation of new technologies for its production, and its adaptability to different fields of application in the construction industry. Despite the excellent properties, the nature of a precursor such as FA (energy industry by-product) implies that its composition is variable, both chemically and mineralogically, which makes it difficult to standardize the activation process in order to obtain specific mechani-

cal properties and durability. Additionally, it should be considered that there is a limited production of these by-products worldwide ($500 - 700$ ton/year), which limits the amount of OPC that could be replaced. It is estimated that by 2030, the worldwide demand for OPC will increase by 216 %, while for FA, only 15 % is projected [39]. Therefore, the study of multi-component cement is necessary, and a blended cement product of an AAC and Portland cement represents a solution to overcome the limitations in terms of the amount of precursor available, as they combine the positive effects of both OPC and AAC.

In a composite material such as concrete, at the microscopic level, the complexity of its structure is evident, since the phases of concrete are not homogeneously distributed among themselves, nor are they homogeneous in themselves. The unique characteristics of the microstructure of concrete could be summarized as follows: first, the ITZ, which represents a thin region next to the aggregate particles, this zone is generally weaker than the rest of the constituent phases of the material. Therefore, it exerts a more significant influence on the mechanical behavior of concrete than its size reflects. Second, each of the phases has a multiphase character; for example, each phase contains different minerals, microcracks, and pores, in addition to a heterogeneous distribution and different solid phases (for the case of the cement paste). Third, unlike other engineering materials, the microstructure of concrete is not an intrinsic characteristic of the material because its components, namely hydrated cement paste and ITZ, are subject to change with time, humidity and temperature [40]. The properties of the microstructure of this material and the distribution of its phases control properties such as strength, elasticity, shrinkage, deformation, workability, cracking, and durability, so microstructure understanding is relevant to know the physical and mechanical behavior of concrete and becomes more significant when dealing with LWAC with a modified cementitious material.

This research project focuses on the effect of partially replacing cement and aggregates in conventional concrete with AAC and LWA to determine the effect on the ITZ and mechanical behavior and the correlation between those two variables. In this way, the following objectives have been proposed.

1.3. Objectives

1.3.1. General Objective

To determine the effect on ITZ and compressive strength of replacing cement and aggregates in conventional concrete with AAC and LWA.

1.3.2. Specific Objectives

- To determine the effect of cement and aggregate substitution in conventional concrete with AAC and LWA on the compressive strength.
- To determine the effect of cement and aggregates substitution in conventional concrete by AAC and LWA on the ITZ.
- To correlate the microstructural development of the ITZ with the compressive strength in conventional concrete with cement and aggregates substitution by AAC and LWA.

2 Chapter 2: Background Information

According to the bibliographic review developed, this chapter presents some theoretical bases that support the purpose of the research. It will begin with a general context about LWAC, its uses, standards, and the principal limitation of its industrial use. Then, the interfacial transition zone (ITZ) problem in LWAC and the behavior of the ITZ with an alternative cementitious matrix. The literature review presents the following highlights: firstly, the ITZ is a thin region between the aggregate and the cement paste in concrete, and it is the weakest part of the concrete and is often the site of cracks. Secondly, the properties of the ITZ could be improved by using lightweight aggregates that have a high specific surface area and a rough surface texture. This chapter concludes by discussing the need for further research on the use of lightweight aggregates and polymers in LWAC.

LWAC have been used for more than two thousand years. The primary references that could be cited are the constructions made during the Roman Empire. Unfortunately, after its collapse, the use of this material was limited due to the low availability and variability of natural lightweight aggregates. Subsequently, developing and producing industrialized lightweight aggregates in the 19^{th} and 20^{th} centuries marked a historical turning point for concrete technology [1, 2, 3]. Nowadays, lightweight structural concrete could be 25 % lighter than normal weight concrete, with compressive strength up to 60MPa [3]. ACI 213R-03 [1] and ASTM C 330 [41] define lightweight structural concrete as having a minimum compressive strength of 17.2MPa at 28 days of curing and densities between $1120 - 1920\text{kg/m}^3$. However, Lightweight Concretes (LWCs) refers to those produced with dry densities less than 2000kg/m^3 [4].

There are three main techniques for the production of Lightweight Concrete (LWC): in the first technique, the aim is to limit the fine fraction of a normal weight aggregate to create air-filled pores (*non-fine concrete*); in the second technique, the aim is to include gas bubbles in a cement paste matrix to form a cellular structure containing approximately $30 - 50\,\%$ pores (*foamed concrete*); and the third technique consists of replacing all or part of the natural aggregates with aggregates containing a high proportion of pores (*Lightweight Aggregate Concrete, LWAC*) [2, 4].

The application of LWAC in the construction industry has many advantages, such as a high strength-to-weight ratio, savings in dead load for structural design and foundation, re-

duced risk of damage due to seismic events in a structure; in addition, it has good tensile deformation capacity, thermal and acoustic resistance, low coefficient of thermal expansion, and increased durability [6, 8, 30, 40, 42]. The properties of LWAC are related to aggregates used in concrete, which depend on the material type and its manufacturing process. The density of a LWAC, for example, depends on the volume and type of aggregate it contains [1, 2, 4]. The aggregates used in a LWAC could combine lightened coarse and fine fractions or even lightened coarse material with an appropriate normal weight fine aggregate. Additionally, for an aggregate particle, the amount of water absorbed and the absorption rate depends mainly on the pore volume, the pore distribution within the particle, and the pore structure. The water absorption of aggregates is generally expressed as the oven-dry mass ratio to the aggregate mass after being immersed for 24h. For lightweight aggregates, the value is within the range of $5-45\,\%$ of the dry mass compared to about $0.5-2\,\%$ for conventional aggregates of higher density. Thus, the properties of LWA used in concrete should be studied on a case-by-case basis. According to ACI 213R-03 [1], the main properties of LWA to be studied are, particle size and texture of the aggregates; bulk density, relative density, moisture content, grain size, strength, porosity, and absorption [11].

Despite the diversity of available lightweight aggregates [6], the mechanical properties of LWAC are lower than normal weight concretes (NWC), being affected by the stiffness of the aggregate particles, the water to cement ratio (w/c), cement content, curing age and density [7, 8, 9]. As a results, significant efforts have been devoted to optimizing their dosage and improving their mechanical properties to make them competent against conventional concretes[10, 11, 12, 43].

To understand the reduction of strength due to the incorporation of LWA, it is necessary to highlight that in a composite material such as concrete, on a micrometer scale, it is composed of three main phases, the hydrated cement paste, the aggregate, and the hydrated cement paste near the aggregate particles, which is called the interfacial transition zone (ITZ). These phases' characteristics and distribution in concrete control its physical, mechanical, and durability properties. It should also be recognized that the microstructure of these phases is highly complex because they are not homogeneously distributed among themselves, nor are they homogeneous in themselves. Therefore, as a lightweight aggregate replaces the natural aggregate, the compressive strength of the concrete is reduced due to the lower intrinsic strength of the lightweight aggregates [1, 2, 4, 11, 44].

2.1. The interfacial transition zone in LWAC

In particular, ITZ has two primary components in its microstructure, as shown **Figure 2-1**: a thin layer of oriented calcium hydroxide (CH), with a thickness of approximately 0.5μm towards the aggregate side, and a thin Calcium silicate Hydrate (C-S-H) gel layer,

with a thickness of approximately 0.5μm towards the paste side. This double layer is known as a *duplex film* and has a total thickness of approximately 1μm. Further away from the aggregates is the main interface zone, between 20μm and 50μm thick, containing cement hydration products with larger CH but smaller than those of any hydrated cement paste [2, 44, 45].

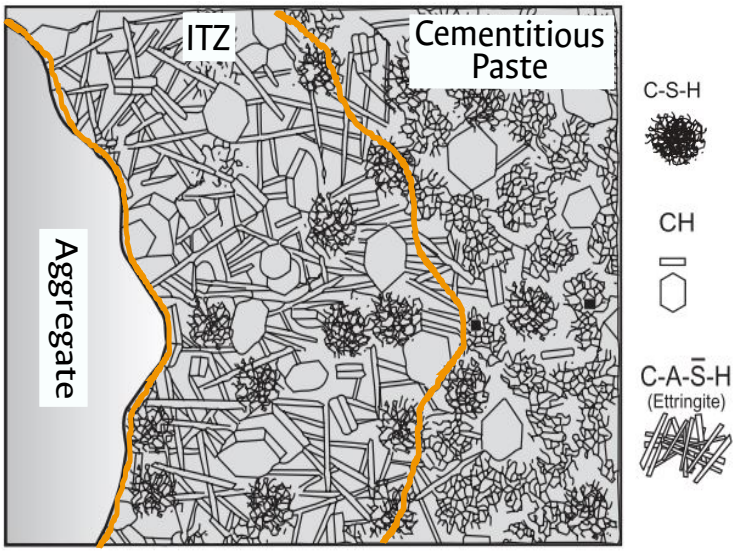

Figure 2-1: Graphical representation of the ITZ. Own source.

The microstructure of ITZ is highly influenced by the formation of the duplex layer, in which the cement particles are unable to bond closely with the relatively large aggregate particles; consequently, the hardened cement paste in ITZ has much higher porosity (2 to 3 times) than the rest of the paste [2]. In 1990, Zhang et al. [43] observed that the thickness of the ITZ corresponds closely to the average diameter of the cement particles. The thickness of ITZ is the distance over which porosity is more significant, at least by 10 % than the paste. The sum of the individual zones generates a considerable volume, to the extent that the total volume of the ITZ is between one-third and one-half of the total volume of the hardened cement paste [2].

According to previous research, it is possible to state that the microstructure of LWAC depends mainly on the nature of the aggregate. Vargas et al. [11] analyzed the microstructure and thickness of the ITZ in concrete made with OPC cement and lightweight aggregates to determine their properties' influence on the concrete. By characterizing the ITZ in LWAC with pumice (pumice) and expanded clays (Aliven), it was concluded that the densification of the ITZ, which refers to its low porosity and higher amount of hydrated phases, could be attributed to the physical and chemical properties of the lightweight aggregate structure such as surface porosity, chemical composition, and degree of crystallinity of the aggregate.

In addition, the aggregate, due to its porous characteristics, has a lower stiffness, and when subjected to a load, it suddenly breaks hence the fragility observed in this type of material [2, 11, 46, 47].

On the other hand, Brooks et al. [48], using fly ash hollow spheres (FAC) to lighten mortars, report an increase in compressive strength when increasing FAC content. Concrete's microstructure modified with FAC is more compact and uniform, which influences its mechanical strength due to a filler effect of the tiny particles and a pozzolanic reaction between a fraction of the FAC and the cementitious matrix; however, in this study, this reaction has not proven. Hanif et al.[49], by thermogravimetric analysis (TGA) and scanning electron microscopy (SEM), identified partially consumed asphalts, which is attributed to a partial reactivity due to the presence of amorphous silica and calcium hydroxide. This reaction produces higher amounts of C−S−H gel in the hydrated cement paste, responsible for the microstructure characteristics described by Brooks et al. [48]. Various materials have been used to lighten concretes and mortars; Muñoz-Ruiperez et al.[50] used concrete and demolition waste to manufacture masonry mortars. In this study, the behavior of these aggregates was found to be inferior to that of natural aggregates. However, fine aggregates obtained from recycled concrete performed better than aggregate from demolition. Brooks et al. [48], on the other hand, used expanded polystyrene (EPS), thermoplastic microspheres (ETM), and glass microspheres (HGM) to lighten mortars, Sengul et al.[51] and Angelin et al. [52], used perlite and expanded clays to lighten concrete. All three investigations used different particle sizes, reducing the compressive strength significantly while reducing the density of the resulting material; this is in agreement with several previous studies [8, 53, 54, 55].

A well-known fact is that the mechanical properties of cement-based materials are highly dependent on the material's structure at the micrometer or nanometer scale. Because of this, it is essential to investigate the microstructure properties of cement-based materials to improve their mechanical performance (e.g., mechanical strength, durability, and density). Furthermore, the most significant challenges are presented at the interface between cementitious matrix and aggregate since this area is responsible for transmitting stresses to the aggregate, ultimately leading to material failure [56].

Many investigations have been carried out to determine the effect of incorporating various polymeric wastes in conventional mortars and concretes. According to the literature review, polymers have had two main uses in the concrete industry: the first as aggregates to substitute natural aggregates and the second as fibers for producing reinforced concrete [57]. The fresh and hardened properties of concrete including polymeric materials have been determined in several previous studies [8, 32, 42, 48, 58, 59, 60, 61].

However, few of them has related mechanical properties to the microstructure characteris-

tics of the resulting material. Brooks et al.[48] report regarding the morphology of polymer-lightened mortar (see **Figure 2-2**) that EPS beads act mainly as weak points in the mortar, promoting the initiation and propagation of cracks in the mortar structure. A similar situation occurs for ETMs, although the particles are smaller than EPS. Therefore, as the fraction of these aggregates increases, the strength of both samples decreases continuously. In this research, it is also reported that, between the two specimens, the ETM has a higher compressive strength when the amount of polymer is low, and it is attributed to a lubricating effect given by the ETM particles by reducing the air content in the mortar.

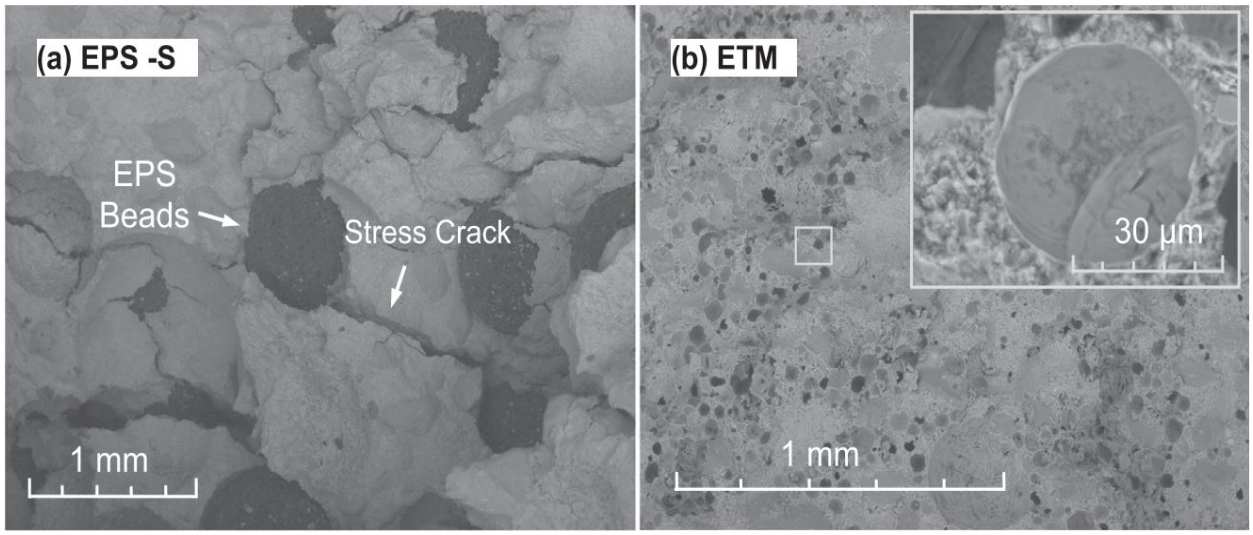

Figure 2-2: Scanning electron microscopy (SEM) showing fracture surfaces in LWAC containing: a) Polystyrene beads (EPS). b) Plastic microspheres (ETM). Taken from: [48]

Subsequently, Bakhshi et al. [62] propose a hypothesis to justify the microstructural behavior due to the incorporation of ultralight polymeric aggregates such as EPS when subjected to loading, taking into account two situations: when in the concrete specimen, its ITZ is almost as strong as its mortar (**Figure 2-3a**) and when the specimen has an ITZ considerably weaker than the paste (**Figure 2-3b**). In the first case, a bigger portion of the first crack path lies in the mortar phase and is also straighter than in the second case. The authors propose that if a fixed volume of EPS beads is added to these two specimens, the stresses would be redistributed more significantly in the concrete microstructure of the **Figure 2-3a**. In the case of cracks passing through the mortar (**Figure 2-3a**), the damaging effect of stress concentration due to the presence of EPS beads becomes more pronounced. Besides, a pure geometrical reason also exists on why EPS beads affect mortar and ITZ differently. As shown in **Figure 2-3c**, since EPS beads are almost spherical and the thickness of ITZ phase is limited, EPS beads could less probably weaken cracks passing through ITZ compared to those passing through mortar. According to the two reasons mentioned, the strength of the

second sample (**Figure 2-3b**) is less sensitive to the presence of EPS beads thus, higher volume contents of EPS are required to create new weaker failure mechanisms. Additionally, taking into account that the bonding with the cementitious matrix is significant in composite materials such as concrete manufacturing; Polymers and organic admixtures must interact with the Portland cement components when they come into contact with water. EPS particles and recycled polymer aggregates generally do not adhere well to dry cement paste because they are hydrophobic, and their surface is electrically charged [63, 64, 65].

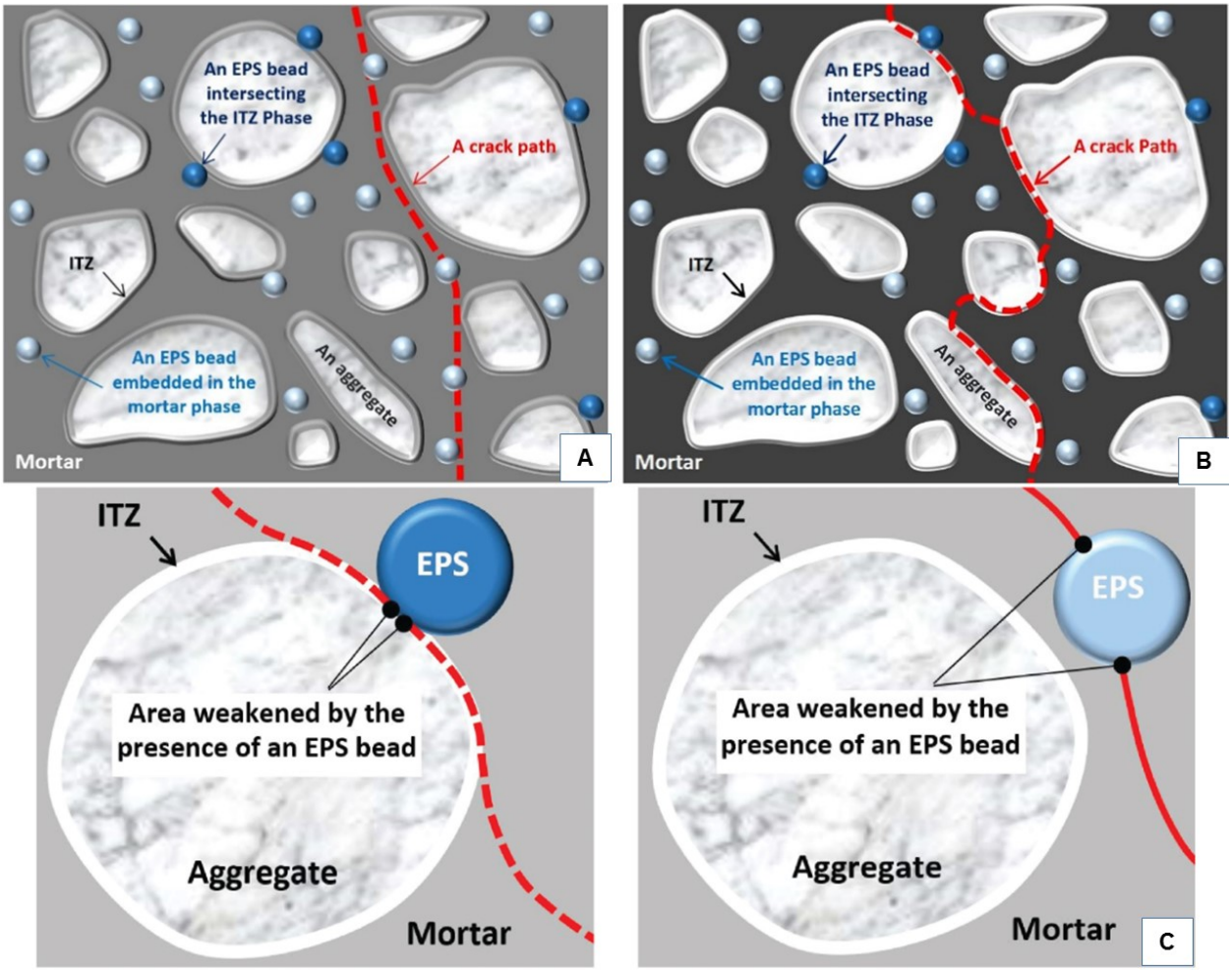

Figure 2-3: Schematic failure plane in: (a) A concrete whose ITZ phase is almost as strong as its mortar. (b) A specimen whose ITZ is considerably weaker than its mortar. (c) Zoom of the failure plane through the ITZ (left) and failure through the polymeric aggregate (right). Adapted from: [62]

Previous research indicated that the compressive strength of polymer-LWAC increases with decreasing polymer aggregate particle size for the same concrete density [8, 58, 66, 67]. Chen et al. [60] confirmed this phenomenon by studying three types of EPS beads with 1.0, 2.5, and 6.3 mm diameter, added to cementitious matrices with different strengths to produce

LWAC. Silica fume was used to improve the material properties. **Figure 2-4a** illustrates the effects of aggregate size on the compressive strength of concrete with different amounts of EPS. It is observed that these graphs start with a drastic negative slope, indicating that high volumes of EPS have a detrimental effect on the compressive strength of concrete.
Additionally, in **Figure 2-4b**, it is observed that the effect of particle size of EPS beads differs as densities and matrix strengths change, indicating that the effect of particle size on compressive strength becomes more significant with increasing EPS. According to Chen et al. [60], this behavior is because lower density concrete generally has a high amount of EPS, which inherently produces a lower strength, so the benefit obtained with the use of smaller particle size was significant. A uniform relationship could then be established between the compressive strength of the concrete and the matrix. In the case of LWAC, the aggregates are usually less resistant and stiffer than the matrix, depending on the LWA density. Therefore, the LWA is decisive for the strength of the LWAC structure [62].

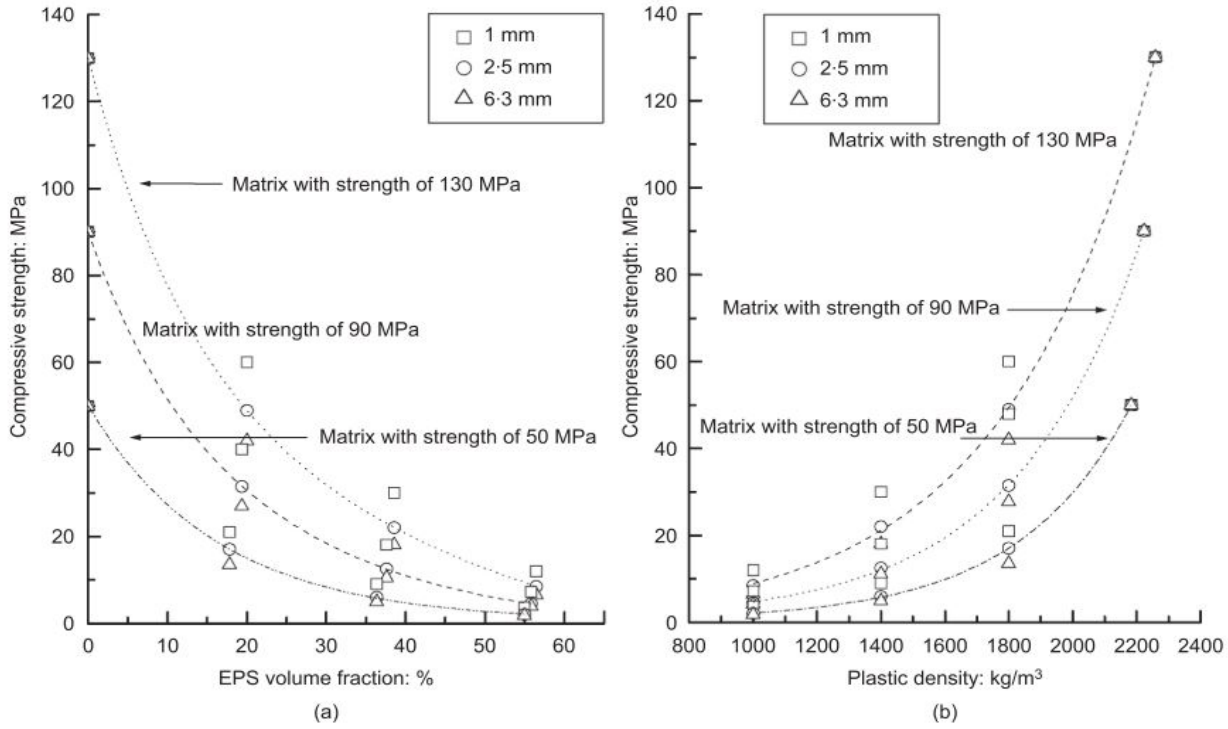

Figure 2-4: Variation of compressive strength and volume percent for different design strengths. Taken from: [60]

Angelin et al. [52] manufactured self-compacting LWACs using partial substitutions of the natural aggregate by two types of lightweight aggregates: tire rubber waste (with a maximum size of 9.5mm and substitutions of 5 %, 10 % and 15 %) and expanded clays (maximum sizes 4.8 and 9.5mm). The microstructure of the resulting material was analyzed in **Figure 2-5**. In this figure, the mechanical interlocking phenomenon between the aggregate and the

cementitious matrix is observed, increasing the mechanical strength and durability of the concrete [11, 68]. In waste tire rubber micrograph, no interlocking is observed between the paste and the tire rubber. Consequently, a zone of weakness occurs between the paste and the aggregate surface. Additionally, lower amounts of C-S-H gel and higher amounts of CH are reported, indicating a decrease in the mechanical strength of the resulting material.

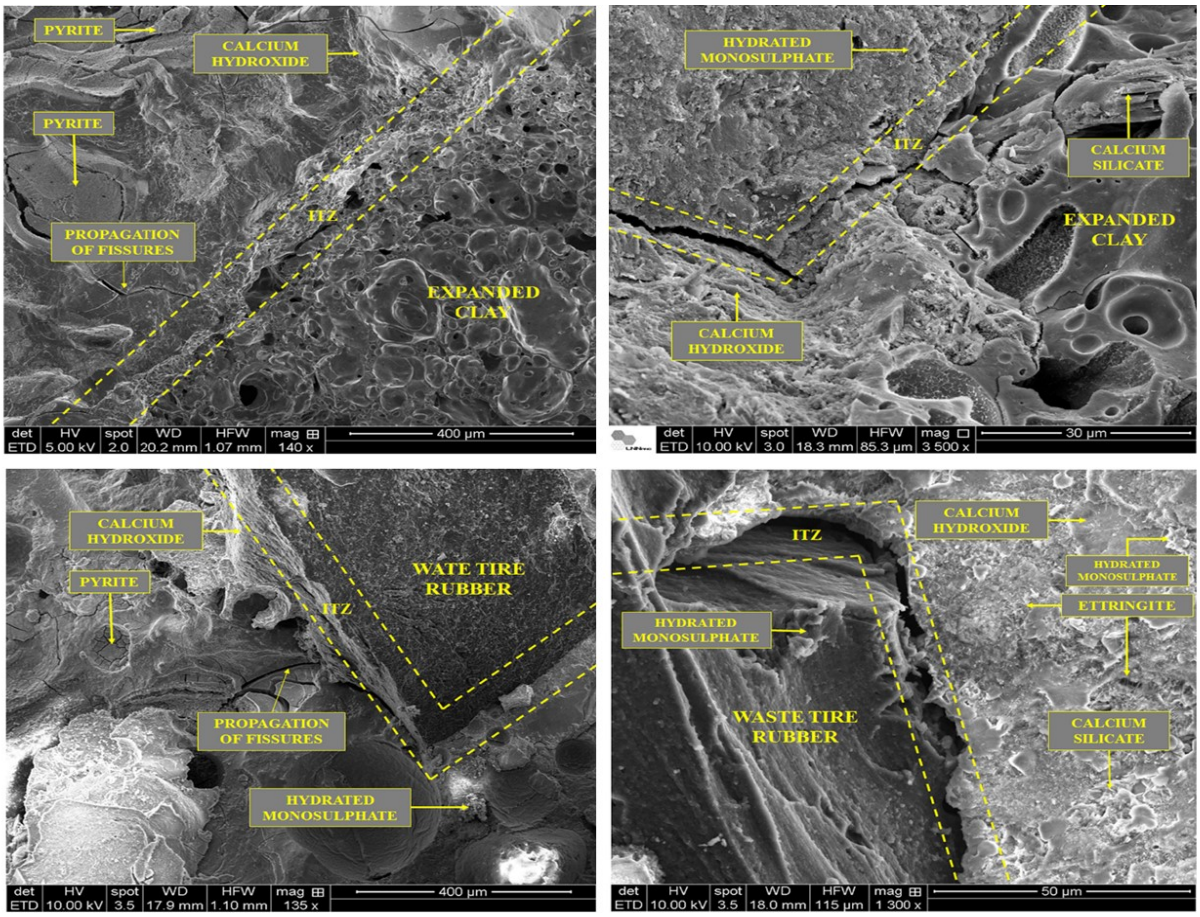

Figure 2-5: Scanning electron microscopy (SEM) for self-compacting concrete with partial substitution of expanded clays and tire rubber residues. Taken from: [52]

Given the production of more significant amounts of CH in these materials, it is feasible to use blended cementitious materials that could achieve excellent performance by adding an alkaline source to accelerate the reaction. These types of cement are part of a line of research that has been developed since 1970, in which a cementitious material is formed from the mixture of two or more types of cement [69, 70], one of which is OPC and fly ash-based alkaline activated cement (AAC). With AAC, a mechanically resistant product is obtained with the reaction between solid material composed of aluminosilicates (such as fly ash) with a solution of an alkaline hydroxide (such as sodium hydroxide); in this process, there is a total or partial transformation of the reactive phase, present in the aluminosilicate,

to a cementitious and compact structure. Using this cementitious material has been a new alternative from the microstructural point of view for LWAC.

2.2. The interfacial transition zone with blended cement

The study and development of AACs have increased due to the possibility of being a variant to OPC since it presents the same or better properties [65, 66]. In the case of fly ash, its reactivity in alkaline-activated blended alkaline cement is much faster and depends on the reaction conditions, particle shape, mineralogy, and particle size. In general, fly ash reactivity increases with increasing glassy phase content [71], particle size reduction [11, 67], and the activator's increasing alkalinity.

Moreover, the ITZ formed in alkaline activated concrete using NWC has totally different features compared to that in OPC concrete. A few studies have discussed the microstructure and properties of ITZ in alkaline activated fly ash (AAFC) concrete and alkaline activated slag (AASC) concrete [70, 72, 73]. Those studies were found that in AAFC there is no apparent weak ITZ near the aggregates due to the formation of sodium aluminosilicate gels (N-A-S-H gels) rather than CH crystals in this region, as is the case in the OPC cementitious matrix [73]. The N-A-S-H gels are the major binding phase in AAFC, which would promote the interparticle bonding and the macroscopic strength in the ITZ. Additionally, the existence of soluble silicates in the initial alkaline solution would also effectively improve the interfacial bonding between aggregates and pastes in AAFC [73]. In AASC, it was observed that the ITZ between aggregates and paste matrix is condensed and uniform, which is attributed to the refinement of pore structure as a result of the filling of reaction products. This is because this zone is mainly composed of N-C-A-S-H or C-A-S-H gels with lower Ca/Si ratio rather than the expansive (Al-free) gels [70]. In recent years, alkali-activated fly ash-slag concrete (AAFSC) as a blended alkali-activated concrete system has been attracted increasing attention because of its potential to provide a good synergy between mechanical properties and durability under ambient curing condition, which could not be achieved by the sole alkaline activated concrete, e.g. AAFC and AASC concrete [72, 74, 75, 76, 77]. Garcia Lodeiro et al. [78] analyzed blended cement activated with solutions of different alkalinity. They found that, although the type of alkaline activator affected the reaction kinetics and the formation of secondary reaction products, it did not seem to affect the nature of the main cementitious gels formed.In a blended cement produced by mixing OPC and a fly ash-based alkaline activated cement (AAC), it is clear that the main reaction products of each coexist, i.e., hydrated calcium silicate (C-S-H) in the OPC and hydrated sodium aluminosilicate (N-A-S-H) in the ash-based AAC.

The high strength and low permeability of LWAC using an alternative cementitious matrix would allow obtaining a low-density concrete or mortar incorporating lightweight aggrega-

tes (LWA) without compromising its mechanical properties and durability. Several research studies have produced LWAC using AAC with different precursors. Posi et al.[79] evaluated the properties of geopolymer concrete using recycled LWA from construction and demolition waste. Huiskes et al. [80] produced a lightweight geopolymer concrete using industrial biowaste as precursor and polyethylene terephthalate (PET) particles as lightweight aggregates. The chemical composition and physical characteristics of the LWA have a significant influence the resulting material properties. For example, Wongsa et al. [81] demonstrated that geopolymer concrete lightened with brick waste has an adequate structural behavior while concrete with the same characteristics lightened with pumice performs more appropriately in manufacturing blocks.

However, the LWAC production with a blended cement has not been reported. Wich has great potential since blended cement is the most expeditious way to achieve OPC substitution, and it has already been demonstrated that LWAC could be made with good performance with each OPC and AAC cement separately. At this point, it is evident that each of the properties of LWA causes changes in the properties of LWAC. Additionally, it should be recognized that the properties of these concrete depend on the characteristics of the cementitious matrix.

2.3. Chapter Summary

Following the findings of the present state of the art, the following preliminary conclusions are presented:

- The compressive strength of cement-based materials is highly dependent on the material's structure at the micrometer or nanometer scale. Because of this, it is essential to investigate the microstructure properties of cement-based materials to improve their mechanical performance. Furthermore, the most significant challenges are presented at the interface between cementitious matrix and aggregate since this area is responsible for transmitting stresses to the aggregate, ultimately leading to material failure.

- The LWAC production with a blended cement has not been reported. Wich has great potential since blended cement is the most expeditious way to achieve OPC substitution, and it has already been demonstrated that LWAC could be made with good performance with each OPC and AAC cement separately The extensive literature review for the consolidation of the state of the art highlights the relevance of the incorporation of lightweight aggregates in large works representing the use of concrete in most of the structure.

- The use of blended cementitious materials is a feasible option for achieving excellent performance in LWAC. These materials are formed from the mixture of two or mo-

re types of cement, one of which is OPC and fly ash-based alkaline activated cement (AAC). AAC is a mechanically resistant product that is obtained with the reaction between solid material composed of aluminosilicates (such as fly ash) with a solution of an alkaline hydroxide (such as sodium hydroxide). In this process, there is a total or partial transformation of the reactive phase, present in the aluminosilicate, to a cementitious and compact structure. Using this cementitious material has been a new alternative from the microstructural point of view for LWAC. This material is a promising new technology for the production of high-performance LWAC because it has been shown to have improved mechanical behavior, durability, and resistance to chemical attack compared to conventional LWAC. It also could be used as an alternative to reduce the environmental impact of LWAC production by reducing the amount of cement required.

- However, like other similar technologies, it requires a gradual process of incorporation and continuous scientific and industrial development. Factors related to durability, such as permeability, have been little studied, according to some research, since the focus of studies tends to center on mechanical properties. Therefore, the properties of expanded clay and expanded polystyrene could be studied in greater depth and in the long term.

3 Chapter 3: Experimental Program

An overview of raw material procurement, cementitious synthesis, design of experiments, instrumental techniques, and characterization of the raw materials is presented in this section. Based on state of the art, the experimental program is proposed in the corresponding stages according to **table 3-1**.

Table 3-1: Summary of stages and methodological activities.

Stage	Activity	Specific Objective
Stage 1: Experimental Set-up.	■ Characterization of raw materials using instrumental analysis techniques. ▪ Identification of experimental design.	■ To know the fundamental characteristics of the materials to be worked. ▪ Identify the variables and the effects on the mixtures.
Stage 2: Design and preparation of concrete mixes.	■ Preparation of lightweight concrete. Curing samples for 7 and 28 days. ▪ Compressive strength test. Selection of best behavior sample. ▪ Preparation, curing, and compressive strength test to complementary sample.	■ Specific Objective 1.
Stage 3: Evaluation of lightweight concrete properties.	■ Thickness measurement of the ITZ by microscopy. ▪ Characterization of the ITZ microstructure.	■ Specific Objective 2. ▪ Specific Objective 3.

In the first stage of this research, the experimental set-up was carried out, characterizing the raw materials employing different instrumental techniques, which will be mentioned later on, to identify the physical properties and fundamental characteristics of the materials to be worked and to identify the main variables and effects on the mixtures. The experimental design that will later allow the analysis of the results was also proposed. In the second stage of this project, the study specimens were elaborated by determining the adequate

quantities of materials in the concrete mix according to the experimental design. Samples were prepared, demolded, and cured at 7^{th} and 28^{th} days. From this stage, one concrete mix where selected according to its mechanical performance to prepare a complimentary sample that was analyzed with advanced characterization techniques. This complementary sample was compared with an LWAC made with OPC by performing the compressive strength test. In this stage, the first specific objective was executed. For the final stage of this research, the two remaining specific objectives were executed, measuring the porosity of the ITZ and correlating these two variables to evaluate the influence of the microstructure of the ITZ on the mechanical properties of lightweight concrete and to determine the effect of the substitution of OPC and conventional aggregates by AAC and LWA on the compressive strength.

3.1. Materials

3.1.1. Aggregates

This research used a mix of lightweight aggregates and conventional aggregates. Its general characteristics are presented below. *The Expanded clays (EC)* are made from clays that exhibit a naturally expansive behavior when subjected to temperatures above 1200°C. Due to the effect of the temperature, the surface layer vitrifies, and gas bubbles are trapped inside. Once cooled, light material is obtained, with a sometimes smooth surface and spherical shape; they have a closed and not very porous outer surface, in contrast to the interior, which is very porous and black [50, 44]. Expanded clays with a maximum size of 9.53mm were used for this research, These materials were obtain from a local company dedicated to the manufacturing and marketing of products for the construction industry, agriculture, and energy sector. *Thermoplastic wastes (EPS)* obtained from a local recycling plant and transformed by mechanical crushing to reach a maximum size of 4.75mm, as reported by previous studies, to obtain the highest compressive strength [48, 60]. A *conventional aggregate (NWA)* with a maximum particle size of 9.53mm was obtained.

To reduce the incidence of coarse aggregates in the microstructure of the samples as much as possible *Fuller-Thompson methodology*, was used for particle size standardization considering the following equation and a maximum particle size of 9.53mm:

$$p = 100 \times (\sqrt{\frac{d}{D}})$$

Where,
p - Percentage by weight passing through sieve.
d - Sieve size.
D - Maximum aggregate size.

3.1.2. Cementicious Materials

This research used two cementitious materials types: commercial cement (OPC) and alkaline activated cement (AAC). The general characteristics for the cementitious materials used are presented as follows:

1. *The OPC* is the most widely used cement worldwide. This material is manufactured from limestone, clays, and other materials of similar composition; under a heating process that induces changes in the properties and produces a partial fusion of the initial components. Partial melting at high temperatures forms tricalcium silicates (C_3S), dicalcium silicates (C_2S), and tricalcium aluminates (C_3A). High early-strength cement for structural use from a local cement company was used for this research, corresponding to an ART type, according to NTC 121 (ASTM C1157/C1157M−17).

2. *The alkaline activated cement (AAC)* was composed of *Fly Ash (FA), lime and activator solution.*

   a) The *FA* is a heterogeneous material composed of crystalline and vitreous minerals, with mainly spherical morphology. The coal fly ash used in this research was a by-product of the combustion of sub-bituminous coal for power generation in the local textile company. Some of the conditions recommended for the use of fly ash as a cementitious raw material are that it has a percentage of unburned particles less than 5 %, iron oxide content less than 10 %, a low calcium oxide content, reactive silica content between 40 % and 50 %, percentage of particles with a size less than 45μm greater than 80 % and a high range of vitreous phase [71].

   b) *Industrial calcium hydroxide* or *lime* (Commercial name) is used in this research, with a purity degree of 95 %. Lime is the product of the hydration of calcium oxide from calcareous or dolomitic rocks subjected to calcination [82]. The reaction is as follows:

   $$CaO + H_2O = Ca(OH)_2$$

   c) *Sodium hydroxide (SH)*, and *sodium silicate (SS)* were used as *activator solution* for the AAC. The SH is manufactured primarily via chloralkali. Its solubility of 20mol/kg water at 25°C makes it a good candidate for use in alkaline activation, as it is one of the highest compared to other alkaline hydroxides. Considering its highly corrosive nature, viscosity and heat released from dissolution are essential properties. SH has shown much lower viscosities than, for example, alkali silicate solutions under similar conditions, favoring the workability of cement pastes [77, 83, 84]. During the alkaline activation of fly ash, SH controls and affects the ordering, during the dissolution process, of the ions that form the new gels and

directs the structure's growth during the gel's hardening and the possible formation of crystals [77, 83, 84, 85]. For this research, an 8M solution was obtained from SH flakes with a purity degree of 99 %. The SS or *Waterglass* comes from the chemical family of Silicates, the generic name of a series of compounds with the formula ($M_2O.nSiO_2$). Its properties are susceptible to its composition and storage conditions. It has been reported in several investigations that soluble alkaline silicates are the most effective activators for most alkaline-activated cementitious materials. SS will raise the Si/Al ratio, giving better mechanical strengths [77, 83]. In this research, the SS used is composed of 8.4 % Na_2O, 27.8 % SiO_2 and, density 1.355g/mL. It was used in a concentration 4.2M. The water used to prepare the solutions is potable water subjected to deionization. This is a process by which, through ion exchange, water undergoes demineralization of ions such as sodium, calcium, iron, carbonates, and chlorine, among others.

3.2. Experimental Design

3.2.1. Statistical Design DoE

A 2×2^3 complete factorial design and block in 2 were proposed. Additionally, four central points were included, and four replicates were considered for the statistical analysis of the results. The first two factors were proposed taking into account their effects on the performance of the AAC, such as the substitution percentages of FA and lime. The third factor considered within the DoE is the combination of lightweight aggregates to identify a proportion of EPS and EC that will achieve the highest compressive strength. Finally, the curing temperature is considered as a block in the DoE. Two working temperatures were used 45°C for three days [86, 87, 82] and ambient conditions until the time of testing. A summary is presented in **Figure 3-1**.

As reported by previous research, for the experimental design first factor, FA replacement percentage, the levels 40 % and 80 % were selected. With a central point in 65 % [23, 86, 88, 89]. The second factor, Lime replacement percentage, 0 % and 10 %, with a center point in 5 % [71, 87, 82, 90, 91]. This research used a combination of EPS and EC LWA to replace NWA in concrete partially. Considering the results reported by Gonzalez-Betancur et al., Almeshal et al., Babu et al., Bakshi et al., and Madandoust et al. [8, 15, 19, 42, 62, 92], the lightweight polystyrene aggregate was limited to 0 %, 15 %, and 30 %. The expanded clays were limited to 5 %, 20 %, and 35 % [11, 93]. In that sense, the amount of conventional aggregate will be the remaining percentage in each combination of aggregate to complete 100 % of the total.

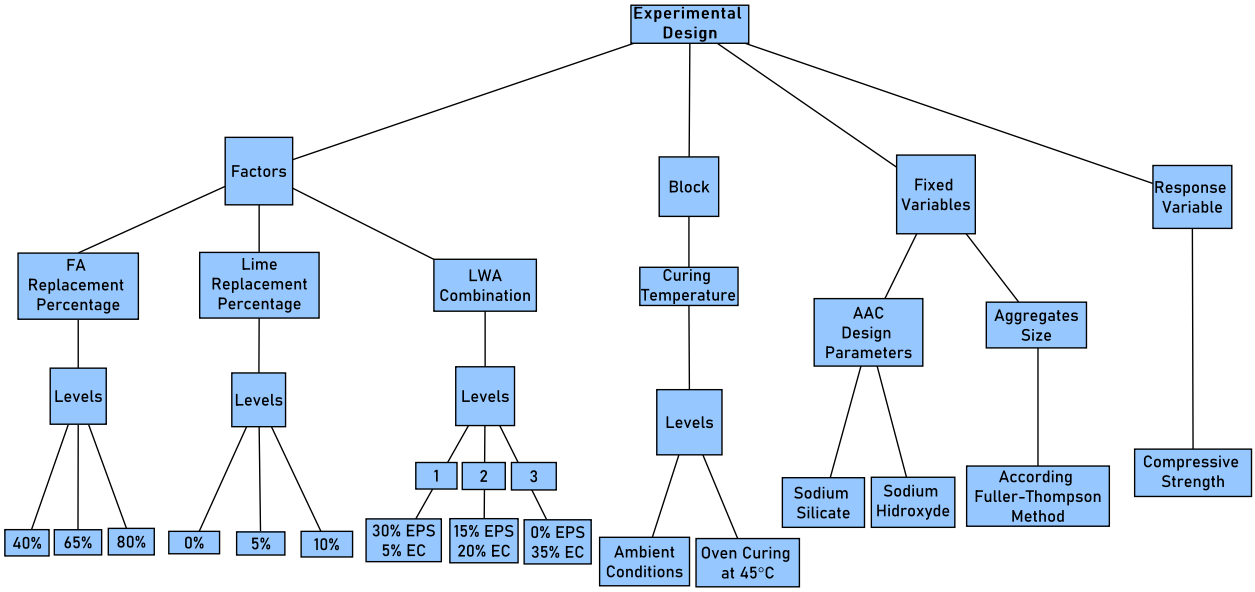

Figure 3-1: Graphical representation of Experimental Design

3.2.2. Complementary Samples

From the DoE proposed, the best compressive strength performance was selected. This means the levels with the best performance concerning the response variable, compressive strength, were selected. A substitution percentage of FA and lime was established to formulate the AAC. A combination of LWA was used to prepare LWAC, with which their microstructural properties were analyzed using advanced characterization techniques. A reference sample was produced with the same LWA combination selected from the DoE. The complementary sample was compared with an LWAC made with OPC.

For microstructural analysis, the samples were obtained from 5cm $\times$ 5cm $\times$ 5cm cubes samples at 28^{th} days of curing. The cube specimen was cut to get a 2cm $\times$ 2cm square transversal section of the sample center using a low-speed diamond saw which is equipped with a wet-cutting system; Isopropanol was used as a lubricant for cutting. After cutting, the sample hydration was stopped by the solvent exchange method. This method removes the free water inside the hardened sample without significantly influencing its microstructure [72, 94]. Herein, the isopropanol solution was used, which is regarded as the best-known solvent to minimize the effects on microstructure and components in cement [95]. The samples were stored in the isopropanol solution for 2 days and then dried in an oven at 40°C until they got constant mass. The square sample was embedded in epoxy resin and well polished.
Blended and OPC pastes were obtained and cured at 28^{th} days for mineralogical and chemical analyses. The process explained above was used to stop the hydration process of the pastes. After hydration was stopped, the samples were ground to a particle size passing No.

200 mesh and stored in Eppendorf tubes.

3.2.3. Concrete Fabrication

The mixtures were prepared considering solids: FA, OPC, and lime. The liquid was formed by: deionized water, SS, and SH [96]. The lime participates by weight substitution in the dosage of the FA used in the alkali-activated cement and both replaced cement. All solids components were homogenized manually in a ball mill. Subsequently, the liquid part was prepared by dissolving caustic soda in deionized water using a magnetic stirrer until the solution reached room temperature. A 0.49 liquid-by-solid ratio (L/S) was used for all the mixes evaluated. The amount of aggregate by absolute volume was also obtained. Once the cement paste was prepared, the corresponding aggregate volume was added, and the mixture was homogenized and compacted in molds. The specimens were cured in an airtight container at an average relative humidity of 98 %. Previous research on the activation of AAC cement determined the curing time at working temperature [87]. Two working temperatures were used 45°C for three days [86, 87, 82] and ambient conditions until the time of testing. Once this time was over, samples were taken to a curing chamber, preserving room temperature and humidity 98 % until the moment of the test.
The mix design methodology proposed by Pavithra et al. [96] was used to calculate the mixing ratios. Mix proportions for some mixes fabricated in this study are presented in **Table 3-2**:

Table 3-2: Mix proportions.

Mix type	%Binder Composition			OPC	FA	Lime	L/S	SH	SS	Water	% Aggregate Composition			NWA	EPS LWA	EC LWA
	OPC	FA	Lime	(g)	(g)	(g)		(g)	(g)	(g)	NWA	EPS	EC	(g)	(g)	(g)
OPC	100 %	0 %	0 %	897	–	–	0.49	–	–	439.5	65 %	15 %	20 %	798.5	184.3	245.7
Blended 1	60 %	40 %	0 %	538.2.	358.8	–	0.49	287.5	152.2	–	65 %	30 %	5 %	798.5	368.6	61.4
Blended 2	30 %	65 %	5 %	269.1	583.1	44.8	0.49	287.5	152.2	–	65 %	15 %	20 %	798.5	184.3	245.7
Blended 3	10 %	80 %	10 %	89.7	717.6	89.7	0.49	287.5	152.2	–	65 %	0 %	35 %	798.5	–	430

3.2.4. Characterization Methods

Physical characterization: *BET test* was used to determine the specific surface area of the materials; *DTP particle size distribution* by sieving the different aggregates according to Colombian technical standards NTC 77:2018 (ASTM C 136:2014) and by laser granulometry on a Mastersizer 2000 for cementitious materials. Aggregate density and absorption NTC 4045:2019 (ASTM C 330:2017) and cementitious materials' density were determined regarding NTC 221:2019 (ASTM C188:2017). This standard explains how to measure the density of hydraulic cement.

Mineralogical characterization: This research used *X-Ray Diffraction (XRD)*, Panalytical X Pert PRO MPD, to determine the crystalline phases and to identify possible chemical reactions between the aggregates and the hydration products of the cementitious material. The following parameters were used: Step $5 - 70°2\theta$; average time by step 60s; step size $0.026°2\theta$; Scan speed $0.111°/s$. A copper anode with $K\alpha = 1.5406\mathring{A}$ was used. *Fourier Transform Infrared Spectroscopy (FTIR)* is a technique that identifies the presence of high or low Si or Al contents, where the tendency to form gels due to the effect of alkaline activation could be observed. All samples were subjected to an infrared beam in transmission mode. The number of scans was 64, with a $4cm^{-1}$ spectral resolution. Formed pellets were fabricated at a total pressure of 10ton, composed of 1mg of sample (with a particle size of approximately 75μm) mixed with 100mg of dry KBr. The recording was performed mid-infrared (between $4000cm^{-1} - 400cm^{-1}$).

Chemical characterization: It was performed by *X-Ray Fluorescence* (XRF), which makes it possible to quantify the chemical composition expressed in components present in the raw materials according to NTC 184:2019 (ASTM C 114:2018). The amount of unburned ash was also determined based on ASTM D 3174:2018. *The glassy phase content* of FA was determined by attacking it with 1 % HF for six hours. The test aims to dissolve the glassy phase of the ash and quantify the crystalline phases. After this attack, the sample is filtered and washed with water to neutral pH. The filter paper is calcined at 1000°C for one hour, obtaining the glassy phase percentage [97]. *The reactive silica content* for FA was determined from the UNE 80225:2012 standard. This standard defines the reactive silicon dioxide (SiO_2) content in Portland clinker base cement, pozzolans, and FA. The sample was subjected to treatment with hydrochloric acid and potassium hydroxide solution. The liquids filtered to determine the glassy phase content in the FA were analyzed by *atomic spectroscopy* (ICP) to determine the elemental composition of the dissolved ions and to establish the amount of reactive alumina. Data recording was performed with a plasma flow rate of 15.00L/min, a nebulizer flow rate of 0.85L/min, a reading time of 5 seconds, and a torch height of 12mm. The detection limits of the equipment for Al and Si atoms are 0.018 and 0.069ppm, respectively.

Mechanical test It is a property widely sought after in cementitious phases, and most articles on this subject define it as a response variable. Nevertheless, measuring mechanical compressive strength is of great utility for materials in different applications in the construction industry. Due to the wide variety of product sizes, geometries, and strength testing equipment, strength results are generally not directly comparable between different research groups or authors in the same research. For this reason, NTC 673:2021 (ASTM C 39M:2021) is defined for samples made for experimental design, 600mm in diameter and 120mm in height cylinder molds. The NTC 220:2017 (ASTM C 109M:2016) might be used for 50mm cubes prepared for the complementary samples.

Morphological characterization: ITZ was analyzed by *Backscatering Scanning Electron Microscopy (BSEM)* in a JEOL 5400 to complementary samples. The voltage and vacuum pressure were 15kV and 15Pa. the sample was then gold metalized. Images at 500× magnifications were tested by each type of aggregate. To guarantee the statistics, photographs were taken around random aggregates. It means that, at most, two images were captured for an aggregate. For each kind of specimen, 18 frames of 500× images were collected. Examples of original BSE images are shown in **Figure 3-2a**.

ITZ porosity quantitative analysis: After the BSE images were obtained, a series of image analyses were carried out, which can be divided into four steps: aggregate boundary delineation, pore segmentation, strip delineation, and quantitative analysis [70, 72, 98, 99]. those steps are described below:

- **Aggregate boundary delineation:** To specify the interface between aggregates and paste matrix, it is essential to delineate the boundary of aggregates. However, it is not possible to automatically specify the aggregate boundary due to the close grey scale between aggregates and reaction products in the BSE images and the irregular shape of aggregates (**Figure 3-2a**). The aggregate boundary delineation mainly includes three steps: First, detecting the boundary of aggregate by the triple magnification of the BSEM image to make sure that the boundary between aggregates and paste matrix can be clearly recognized (**Figure 3-2b**). Second, labeling the edge of the aggregate (Figure **Figure 3-2c**). Third, getting rid of the aggregate area by cutting the labeled aggregate (**Figure 3-2d**). Finally, the boundary of aggregate in the whole image was specified.

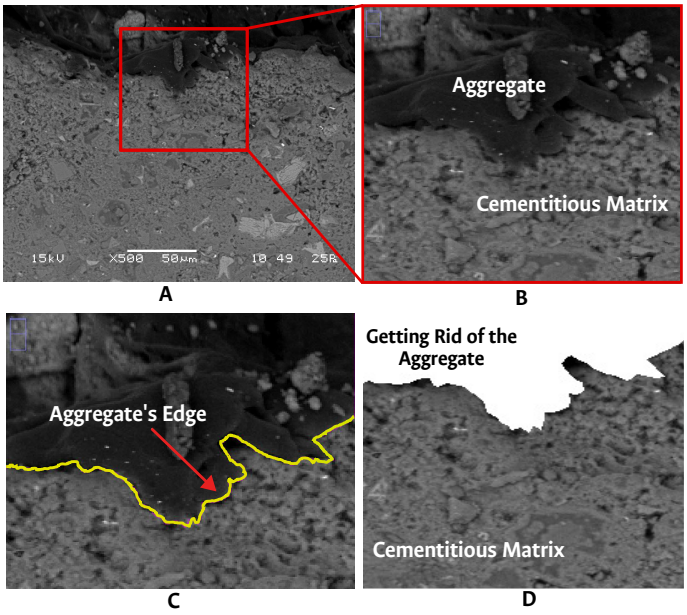

Figure 3-2: Aggregate boundary delineation process.

- **Pore segmentation:** The most crucial characteristic of ITZ in comparison with the bulk paste is its increased porosity. Herein, it should be noted that the term *pores* used here are regarded as a general term for epoxy-filled voids in the sample, which includes capillary pores, cracks, and hollow reaction shells [72, 98, 100]. Determining lower and upper threshold values in the histogram pattern is crucial in grey scale analysis. Unambiguously, the lower threshold can be set equal to zero. As for the upper threshold, the overflow criterion method was chosen [101]. The overflow method is based on the cumulative histogram. A typical frequency counts histogram, and its total area segmented (cumulative curve from the histogram) are shown in **Figure 3-3a,b** respectively.

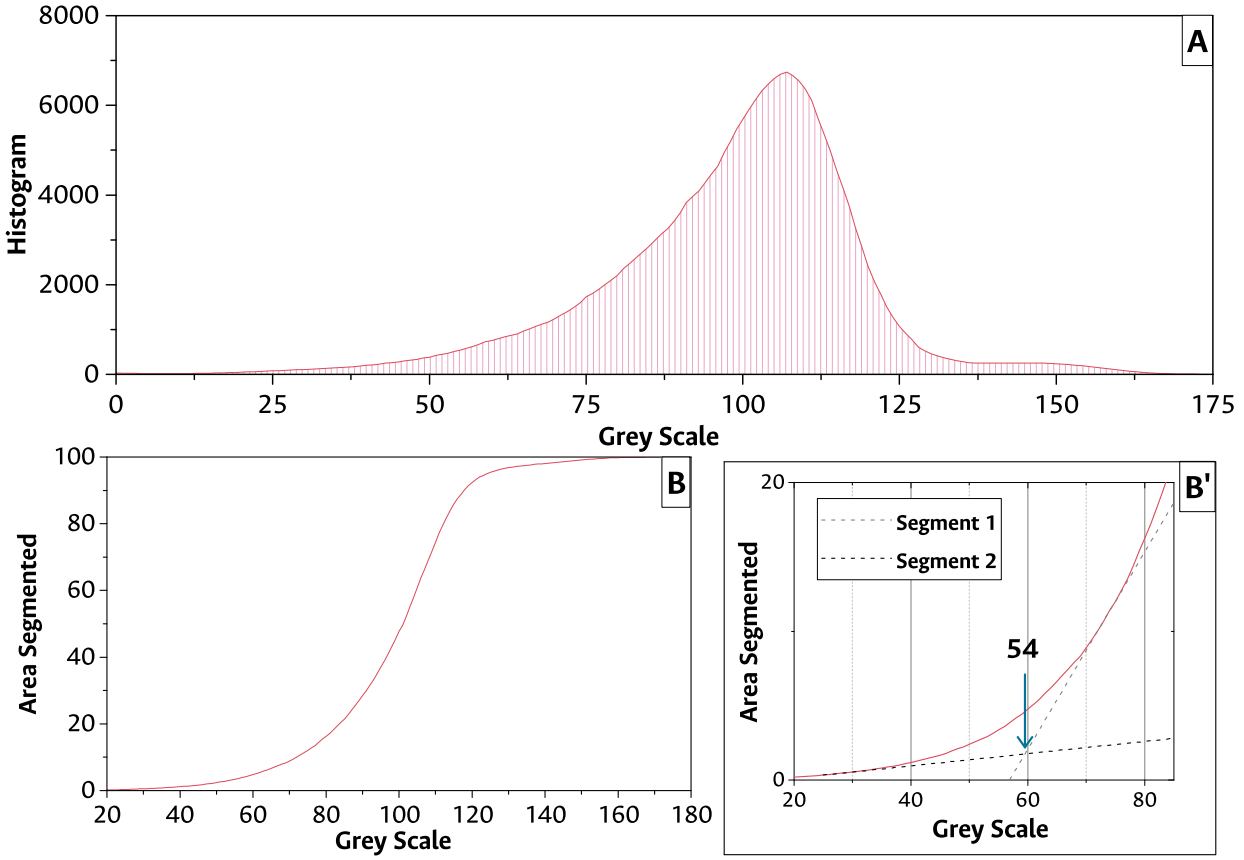

Figure 3-3: Upper threshold values determining process in the histogram pattern.

When the total area segmented is plotted against the threshold level, the critical overflow point corresponds to the inflection of the cumulative curve, which can be estimated from the intersection between the two linear segments, as shown in the **Figure 3-3b'**. The grey value at this intersection can be used as the upper threshold level for porosity. However, this value may slightly overestimate the true overflowing point. A more conservative estimate may be obtained from the

point where the curve begins to deviate from the first linear segment. This can be manually selected or approximated by multiplying the grey value obtained at the intersection with a factor of 0.9 [101].

- **Strip delineation:** To characterize the interfacial properties along the distance from the aggregate surface, successive strips with a specified distance were delineated based on the strip delineation method called concentric expansion [72, 98, 100]. Therefore, 12 successive strips of 5μm width were delineated per image and repeated on 18 images for each specimen. A typical example is shown in **Figure 3-4**. It should be noted that the ITZ width below 5μm cannot be detected.

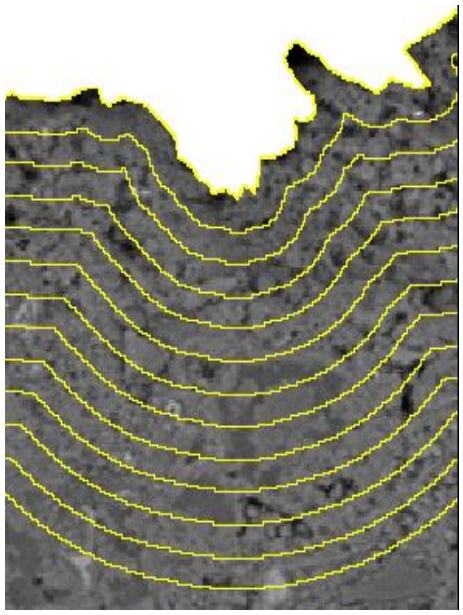

Figure 3-4: Strip delineation process.

- **Quantitative analysis:** The properties of each strip can then be quantified with Image J software assistance. With this quantification technique, is possible to determine the of pores quantity and size of pores to build a cumulative pore size graph. It should be noted that the segmented pores here are assigned to the porous patches with the greyscale below the threshold defined for pores instead of the single pores. The porous patches mainly consist of interconnected capillary pores, microcracks, and hollow shells [72, 102]. This is mainly due to the size limitation of the BSEM images [103].

4 Chapter 4: Results and Analysis

This section discusses the results obtained from the activities proposed in the methodology. The chapter is divided into four sections corresponding to the activities identified in the methodology. The first section is the raw materials characterization, where the principal raw materials properties were obtained through experimental tests. The second and third sections are about the effect of cementitious matrix and LWA replacement on compressive strength and ITZ. According to the methodology presented in the last chapter, the first two specific objectives were done in this section. Lastly, the correlation between ITZ and compressive strength performance is presented to finish the third specific objective of this research project. In addition, at the end of each section, the most relevant results will be presented, which will help the reader fully understand the conclusions drawn.

4.1. Raw Materials characterization

4.1.1. Cementitious materials characterization

The chemical composition of OPC, FA, and lime is shown in **Table 4-1**. In line with this, FA can be classified as type F (NTC 3493:2019/ASTM C 618:2019). The FA composition is acidic since it contains mainly silica and a small amount of calcium [104, 105]. The conventional cement used corresponds to an ART type (NTC 121/ASTM C1157) of high early strength. The density is similar for FA and lime, 2160kg/m^3 and 2143kg/m^3, respectively. In the case of cement, the density is significantly higher. There is a similarity in the specific surface area of cement and FA, corresponding to 504.78m^2/kg and 490.95m^2/kg, respectively.

On the other hand, it is 705.67m^2/kg for lime, a difference concerning the other cementitious materials. The FA presented a reactive silica percentage of 42.20 %, a glassy phase content of 65.71 %, and the amount of reactive alumina was 22.54 %. These values indicate that fly ash presents good characteristics to be alkaline-activated, according to what was reported by other researchers [71]. Industrial lime with 95.6 % of calcium hydroxide and 4 % calcium carbonate content (measured by XRD using the Rietveld method. R_{wp} = 12.5 %) was employed. Finally, sodium hydroxide (SH) was used as Caustic Soda Flakes with a purity of 99 %. The Sodium silicate (SS) available for this research has a Na_2O/SiO_2 ratio of 1:3, with 8.4 % Na_2O and 27.8 % SiO_2 and density of 1366kg/m^3 and the kneading water is

potable properly demineralized.

Table 4-1: Chemical composition of OPC, fly ash, and lime. Determined by XRF. Percentages of oxides by mass

Material	SiO_2	Al_2O_3	CaO	Fe_2O_3	MgO	Na_2O	K_2O	TiO_2	Other	LOI*	ρ (kg/m^3)
OPC	20.51 %	4.66 %	59.49 %	3.15 %	2.72 %	0.29 %	0.29 %	0.33 %	3.13 %	5.43 %	3270
FA	55.26 %	26.95 %	1.00 %	5.66 %	1.78 %	0.44 %	0.75 %	2.28 %	1.51 %	4.37 %	2160
Lime	0.14 %	0.06 %	73.42 %	0.07 %	0.37 %	–	–	–	0.34 %	25.6 %	2143

*LOI Lost by ignition at 950°C. ρ, bulk density.

The particle size distribution is shown in **Figure 4-1** and **Figure 4-2**. For FA, a trimodal distribution is observed with maxima at 0.7μm, 9μm, and 100μm. Sixty percent of the particles have a particle size less than 45μm and this material has a $d_{50} = 30\mu$m. This indicates that FA has a wide range of sizes. In contrast, the cement shows a bimodal distribution with maximum points at 18μm, and 35μm. On the other hand, lime has the finest particle size (90 % of the lime has a particle size of 23μm), and due to its unimodal distribution, it is the most homogeneous raw material.

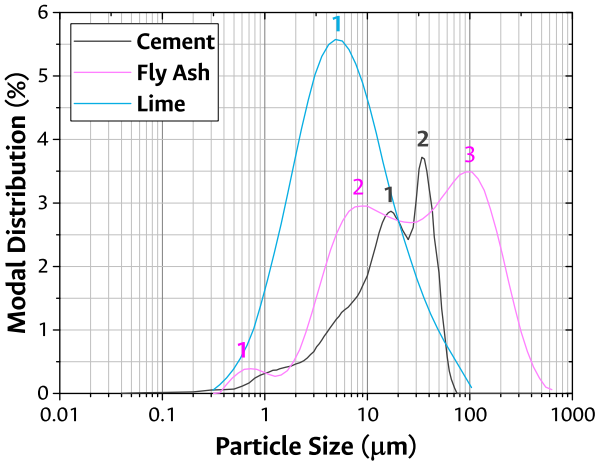

Figure 4-1: Modal size distribution of cement, fly ash and lime.

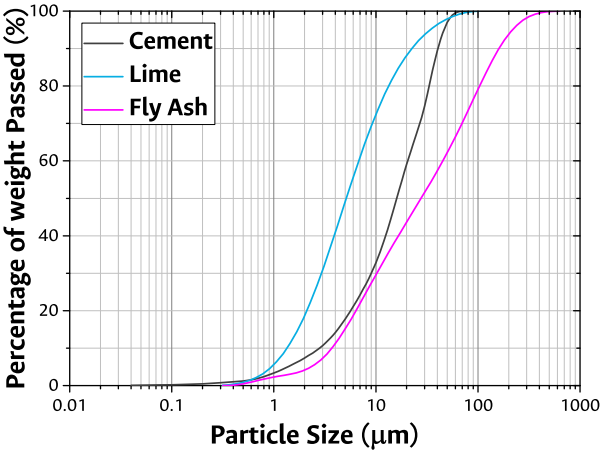

Figure 4-2: Particle size distribution of cement, lime and fly ash.

The **Figure 4-3** shows the qualitative mineralogical composition for FA and lime. The presence of a low degree of crystallinity phase between 2θ values of 20°C to 40°C and three crystalline phases, mullite (M), quartz (Q), and hematite (H), is observed for FA. Portlandite (CH) and calcium carbonate (T) are noticed in lime [82, 87]. The mineralogical composition of the OPC used in this research presents a more amorphous composition than the other raw materials due to the halo observed between $30° - 35° 2\theta$. This material presents the typical mineralogy of an OPC for structural use, with high early strength, due to the intensity

and repetitiveness of the Alite peaks in the diffractogram. In addition, it shows calcium ferroaluminates, and some Belite and gypsum peaks.

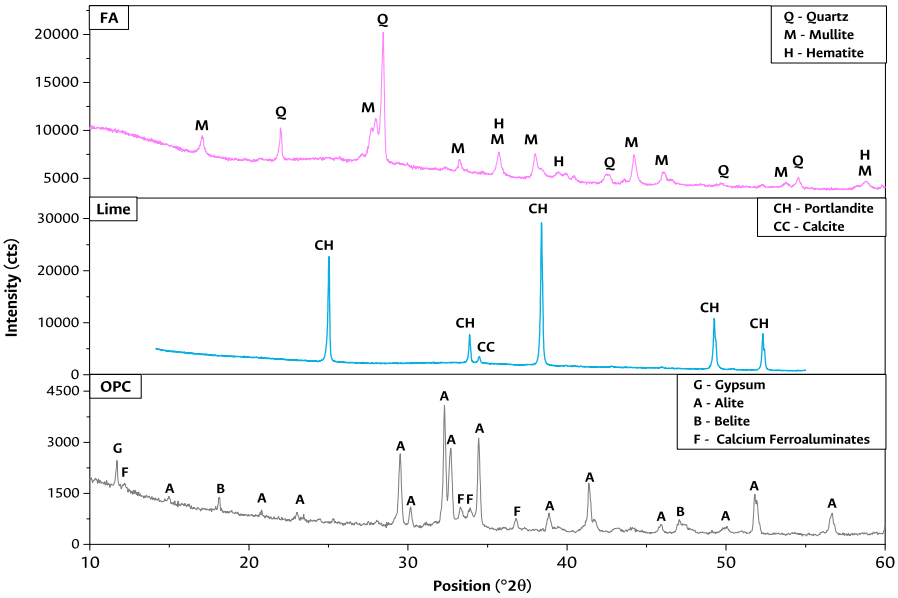

Figure 4-3: Fly ash, lime, and OPC X-Ray diffraction.

4.1.2. Aggregate characterization

Optical micrographs were carried out for morphological characterization of the aggregates and BET testing to determine surface area. Aggregate density (Following NTC 237:2020/ ASTM C 128:2015), humidity and absorption were determined according to Gómez-Cano et al. [106] procedure. The particle size distribution was obtained by sieving according to NTC 77:2018 (ASTM C 136:2014) and NTC 4045:2019 (ASTM C 330:2014). The specific surface area in **Table 4-2** indicates that EC lightweight aggregates have a greater surface area due to their shape, surface roughness, and porosity, validating their angularity and high porosity on their surface [11, 93].

Table 4-2: Aggregate Properties

Aggregate	**Density**(g/cm^3)	**Absorption**(%)	**Surface Area**(m^2/g)
EPS	0.01	0.1 %	-
EC	1.10	17 %	1.89
NWA	2.74	0.70 %	0.78

The NWA packing combines oval, flat, and angular particles. As it is a material with higher specific gravity, the pore size on the surface is small compared to lightweight aggregates.

Therefore it has less roughness, which is observed in the measure of lower surface area. Expanded clay lightweight aggregate has a higher absorption due to its porosity and capillary pore size in its structure, followed by conventional aggregates with a defined crystalline structure and a very dense material with lower porosity. Expanded polystyrene wastes have a lower absorption as their hydrophobic nature [11, 52, 14].

The Optical micrographs carried out for morphological characterizing of the aggregate are shown in **Figure 4-4** and were taken at two different magnifications, 0.75x (**Figures 4-4a,c,e**) and 2x (**Figures 4-4b,d,f**). Expanded clay has a spherical shape (**Figure 4-4a**), and rough surface. Its surface is a brown vitrified layer of variable thickness with less porosity in the center of the material (**Figure 4-4b**). The EPS lightweight aggregate has a spherical shape (**Figures 4-4c**), with a smooth surface. Due to the crushing process it underwent, some semicircular particles are observed with residues of other polystyrene particles adhered to them (**Figure 4-4d**). The conventional aggregate corresponds to crushed gravel with oval rock pebbles (**Figure 4-4e**), angular and rounded shapes, mostly smooth surface, and aphanitic texture observed in **Figure 4-4f**, its structure shows less porosity on the surface when compared to the lightweight aggregates.
Figure 4-5 shows the different particle size curves of LWA and NWA used for this research and, **Figure 4-6** present the Fuller-Thompson method for aggregates standardization. It can be seen that only the NWA (purple line) meets the requirements of retained percentages established by NTC 77:2018 (ASTM C 136M:2014). EC Lightweight aggregate (orange solid line) has a particle size close to fines. It lacks material in the 1/2" and 3/8" (12.5mm−9.5mm) sizes. On the other hand, EPS (green line) is coarser and has a lower percentage retained in the fines zone ($4.76 - 2.36$ mm).
It has been studied that the particle size of lightweight aggregates affects the thickness of the ITZ [107]. In that way, due to aggregates dispersion within the range to be used in lightweight concrete production and to minimize the effect of aggregate size on the ITZ thickness, it was decided to use only the aggregates passing the 3/8"(9.5mm) sieve and retained on the No.16(1.18mm) sieve, excluding those contained on the upper and lower sieves. Besides, the Fuller-Thompson method was used for the packing of aggregate particles. This method was used to obtain the aggregate combination, according to section 3.2.1. **Figure 4-6** present the Fuller-Thompson fitted particle distribution for three aggregate combinations evaluated in this research.

4.1.3. Section Summary

The percentage of variation between OPC and AAC cementitious raw materials density is around 34 %. This could indicate that the cementitious raw materials would also reduce the density of the blended LWAC manufactured. Additionally, the mixing process of FA, lime, and OPC could lead to the formation of a film of lime on the surface of the resulting mix-

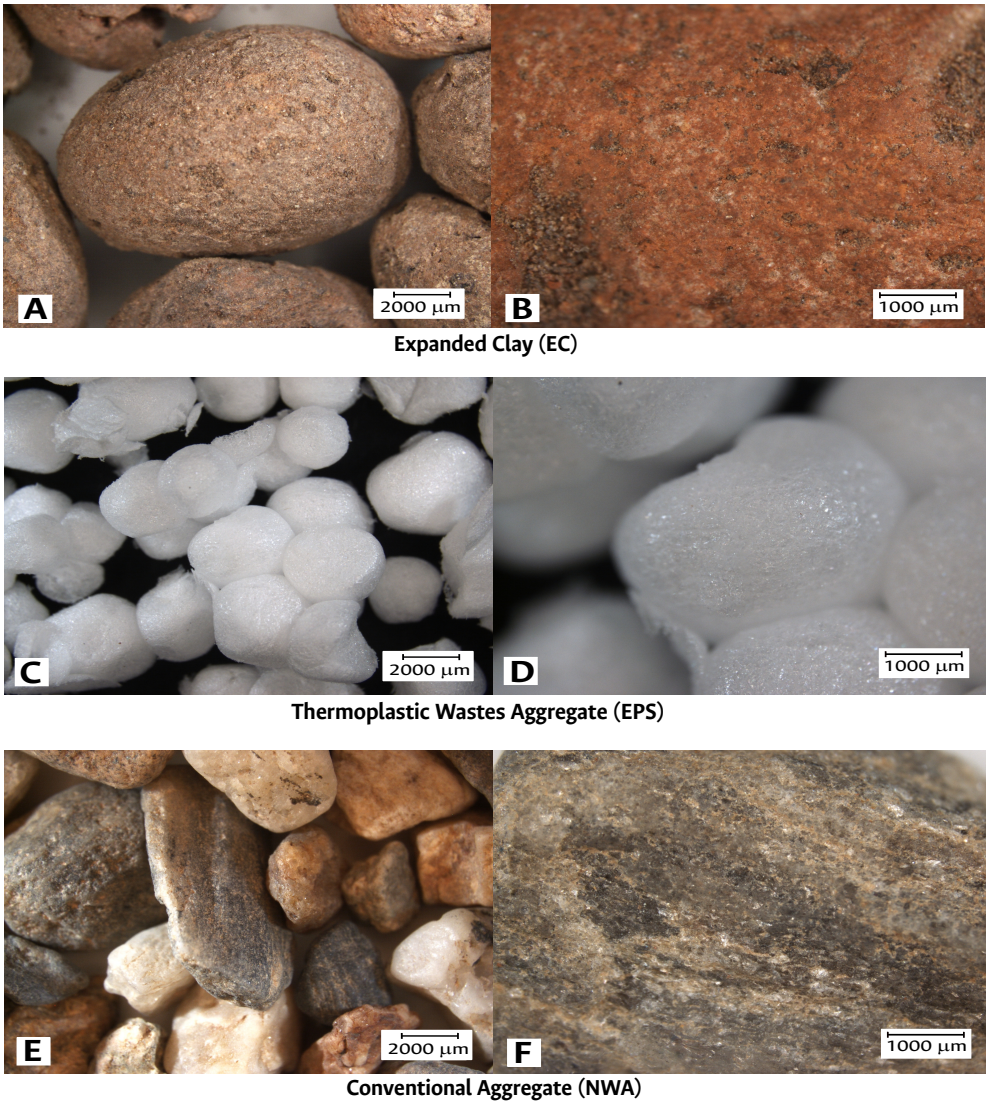

Figure 4-4: Optical micrographs of Aggregates used. Images magnification 0.75x and 2x.

ture, as lime particles are much smaller than FA and OPC particles; this could modify the products obtained in the hydration process.

The expanded clay surface characteristic could react with the activation solution from AAC, generating an ITZ densification and reducing its porosity. The EPS's smooth surface and spherical shape could hinder the adherence between LWA and the cementitious matrix. Furthermore, variations in aggregate absorption and surface area can influence the formation of cementitious gels, generating an activating solution accumulation in the vicinity of the LWA and altering diffusional processes.

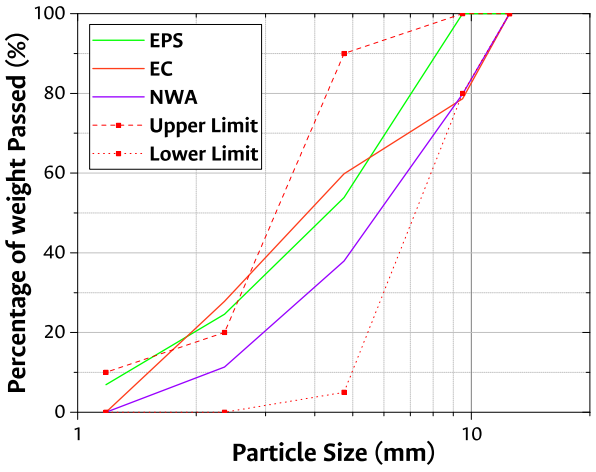

Figure 4-5: EPS, EC, and NWA size particle distribution. Limits (Red dot lines) according to NTC 4045:2019 (ASTM C 330:2014)

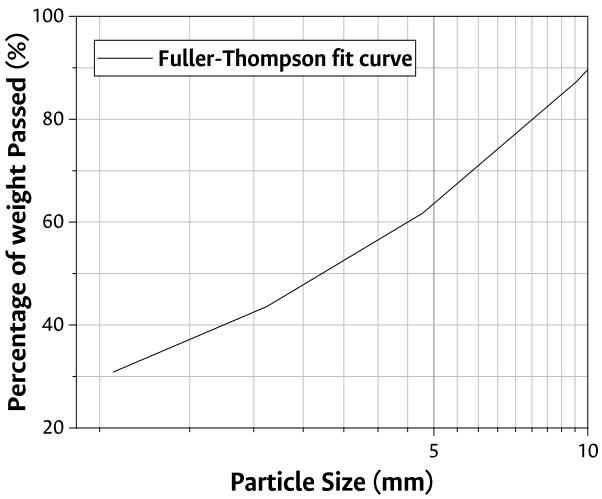

Figure 4-6: Fuller-Thompson fitted particle distribution for three aggregate types evaluated.

4.2. Effect of cementitious matrix and LWA replacement on Compressive Strength

The Pareto diagram for the 7^{th} and 28^{th} days of curing are presented in **Figure 4-7a,b**. The reference line for statistical significance in the Pareto plot is drawn at the quantile $(1-\alpha/2)$ of a t distribution with degrees of freedom equal to the degrees of freedom for the error term. The Pareto diagram graphically identifies the significant treatments within the proposed DoE. At 7^{th} days of curing, in **Figure 4-7a**, the variables that significantly affect compressive strength are the FA replacement percentage (FA), the interaction between FA and lime (FA-Lime), and lime replacement percentage (Lime). In the case of the 28^{th} days of curing, in **Figure 4-7b**, the variables that significantly affect compressive strength are the interaction between FA and lime (FA-Lime), lime replacement percentage (Lime), and the aggregate. In that way, the analysis did not consider the other factors and interactions that are smaller than the pre-established reference line in the Pareto diagram.

The statistical analysis of variance (ANOVA) for the DoE proposed for 7^{th} and 28^{th} days of curing are presented in **Figure 4-7c,d**. For the ANOVA, the null hypothesis is that the means of treatments evaluated have no significant effect on the mechanical compressive strength. In turn, it has no significant impact on the formation of cementitious compounds. For a significance $\alpha = 0.05$, with associated confidence of $\beta = 0.95$, the null hypothesis is rejected if the p-value is less than α. Additionally, the F value in an ANOVA can determine if the means of three or more treatments are different. ANOVA uses the F value to statistically evaluate the equality of means and in this way, determine which treatments are significant

in the model. The results of the statistical analysis for both 7^{th} and 28^{th} days of curing (**Figure 4-7**c,d) indicate that FA replacement percentage, lime replacement percentage, and the double interaction are the most critical factors in improving compressive strength, according to F-values, suggesting that the cementitious matrix dominates the compressive strength developing.

Moreover, The R^2 value is a statistical measure of how close the data are to the fitted regression line obtained by the ANOVA. The higher R^2 value is an indication that the model explains all the variability in the response data around its mean. A high R^2 value and significant factors in the DoE indicate that changes in the predictors are related to changes in the response variable and that their model explains much of the variability in the response. The R^2 values presented in **Figure 4-7c,d** allow the models to explain the data variability with estimates higher than 70 %, ruling out a random behavior of the model. The S-value represents the average distance that the observed values fall from the regression line. Conveniently, it tells you how wrong the regression model is on average using the units of the response variable. Smaller S values indicate that the observations are closer to the fitted line.

The validity of the results obtained in any ANOVA is subject to the assumptions of the DoE being met. These assumptions are normality, homoscedasticity (equal variance of treatments), and independence. The residuals of the ANOVA model should be examined, using diagnostic statistics to determine if the proposed model is adequate and if the regression assumptions are met. This is important since if the model is not adequate, it will misrepresent the data. Tests on residuals were executed, and p-values for each are shown in **Table 4-3**. For the normality assumption, the null hypothesis will be that the ANOVA residues have a normal distribution. For the homoscedasticity assumption, the null hypothesis will be that variances are homogeneous in model residues; and for the independence assumption, the null hypothesis will be that the ANOVA residues are independent since no autocorrelation is found in the model. Anderson-Darling, Barlett, and Durbin-Watson tests were taken to verify the normality, homoscedasticity, and independence assumptions. As all the p-values shown in **Table 4-3** are higher than pre-set α, the model's premises are confirmed to be met.

Table 4-3: Tests results to Verify Assumptions of Linear Model

Statistical Assumption	Test	P-Value 7^{th} curing days	P-Value 28^{th} curing days
Normality	Anderson-Darling	0.718	0.237
Homoscedasticity	Barlett	0.493	0.387
Independence	Durbin-Watson	2.090	1.739

Moreover, the curing temperature effect, which is represented in the model by the block, is not appreciable for 7^{th} days of curing. The OPC hydration could explain this, which is an

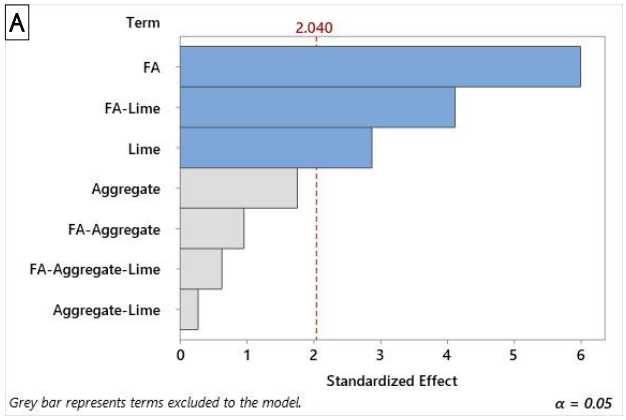

C

Analysis of Variance Table Response: 7 Days Compressive Strength

	DF	Sum.Sq.	Mean Sq.	F-Value	P-Value	R^2	S
Model	4	1055.90	263.972	18.610	0.000		
Lineal Effects	2	627.10	313.534	22.110	0.000		
FA	1	510.00	510.006	35.960	0.000		
Lime	1	117.10	117.063	8.250	0.007	70.60%	3.77
2 Terms Interactions	1	240.30	240.267	16.940	0.000		
FA*Lime	1	240.30	240.267	16.940	0.000		
Curvature	1	188.60	188.552	13.290	0.001		
Error	31	439.70	14.183				
Total	35	1495.60					

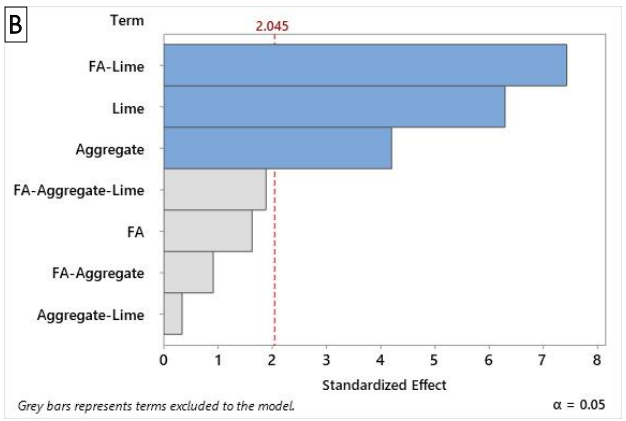

D

Analysis of Variance Table Response: 28 Days Compressive Strength

	DF	Sum.Sq.	Mean Sq.	F-Value	P-Value	R^2	S
Model	6	1099.36	183.227	22.050	0.000		
Block	1	90.59	90.592	10.900	0.003		
Lineal Effects	3	497.27	165.758	19.950	0.000		
FA	1	22.02	22.025	2.650	0.114		
Aggregate	1	146.49	146.486	17.630	0.000	82.02%	2.88
Lime	1	328.74	328.763	39.560	0.000		
2 Terms Interactions	1	458.11	458.106	55.130	0.000		
FA*Lime	1	458.11	458.106	55.130	0.000		
Curvature		53.39	53.389	6.420	0.017		
Error	29	240.99	8.31				
Total	**35**	**1340.35**					

Figure 4-7: Pareto diagram for the effects in DoE (a, b), ANOVA (c, d) Compressive Strength for 7th (a, c) and 28th (b, d) days of curing.

exothermic reaction [108] and will release heat during its hydration. The energy from this hydration heat would promote the polymerization that generates $M-A-S-H$ ($M = Na^+$ or Ca^{2+}) gel for concrete to gain strength [78], making the difference of curing temperatures nonsignificative [78, 90, 109]. At 28^{th} days of curing, curing temperature becomes significant in the model. This could be explained by considering that the concretes' activation temperature was low, similar to the ambient curing in tropical countries. According to literature, the strength acquisition in this condition is slower due to a low reaction gradient [82, 87, 90].

The following analysis of the linear effects of the factors and interactions between them in the DoE, did not take into account the factors and interactions that are greater than the pre-established α value.

Figure 4-8a, represents the linear effect of FA on the DoE for the samples at 7^{th} days of curing. Since the linear effect for this factor at 28^{th} days of curing is not significant because its p-value is higher than the preset α value the results of the mean for this treatment are not shown. The vertical axis represents the average compressive strength, and the horizontal

axis represents the evaluated treatments. Also, the theoretical modulus from the mix design is presented in the **Figure 4-8b**. **Figure 4-8a** shows that the experimental design proposed has a curvature effect in the proportion of 65 % FA.

Considering the $CaO/(SiO_2 + Al_2O_3)$ modulus, the amount of lime for the evaluated treatments decreases as the percentage of FA increases. This will condition the nature of the hydration products formed [109, 110]. Thus, with a higher amount of CaO, products such as (C, A)−S−H would be formed, corresponding to a high-Calcium AAC [87, 111]. Meanwhile, with a lower CaO concentration, $N-A-S-H$ would prevail, as a hydration product corresponding to a low-Calcium AAC [112, 113, 114]; consequently, it will condition the mechanical behavior of the lightweight concretes under study.

A significant reduction in compressive strength can be observed when 80 % FA is added (53.5 % This value is obtained, compared with the central point). A considerable reduction in $CaO/(SiO_2+Al_2O_3)$ modulus from 0.529 to 0.381 is observed (**Figure 4-8b**), which means saturation of SiO_2 in the system, reducing the Si ion mobility. Consequently, difficulting the formation of amorphous aluminosilicate hydrate gel ($N-A-S-H$), the main reaction product of an AAC, based on a low-Calcium FA. Also, no enough Ca is available to produce (C, A)−S−H gel. Furthermore, higher Na_2O/SiO_2 modulus could indicate a lower catalyst concentration, which could be slowing down the Na_2O exchange with CaO to form $C-S-H$ or $C-A-S-H$ gel in the hydration reaction of the AAC material within the blended cement [89, 90, 111].

When the FA replacement percentage is 40 % (**Figure 4-8a**), a reduction in compressive strength is also observed (15.7 % This value is obtained, compared with the central point). In this case, a considerable increase from 0.529 to 1.01, a double increase compared to the central point in $CaO/(SiO_2 + Al_2O_3)$ modulus is observed. This could indicate a CH saturation in a blended cement where the pozzolanic reaction is the principal effect responsible for the compressive strength obtained due to the high concentration of CH from OPC [89, 90, 111, 87].

In **Figure 4-9a**, the lime effect for the 7^{th} and 28^{th} days of curing is presented. The horizontal axis represents the evaluated treatments, and the vertical axis represents the average compressive strength. The treatments evaluated do not present statistically significant differences between 7^{th} and 28^{th} days of curing. However, there are significant differences when the amount of lime is 0 % as regards the other replacement percentages.

Compared to the central point, there was a reduction in compressive strength of 43.8 % for a lime substitution percentage of 0 %. Due to the absence of lime in the system, the system will have as main hydration products the $N-A-S-H$ and the hydration products generated by the percentage of OPC in the mix. Thus, the compressive strength will also depend on the amount of alkali ions present (Na^+) responsible for separating the Al-O and Si-O from

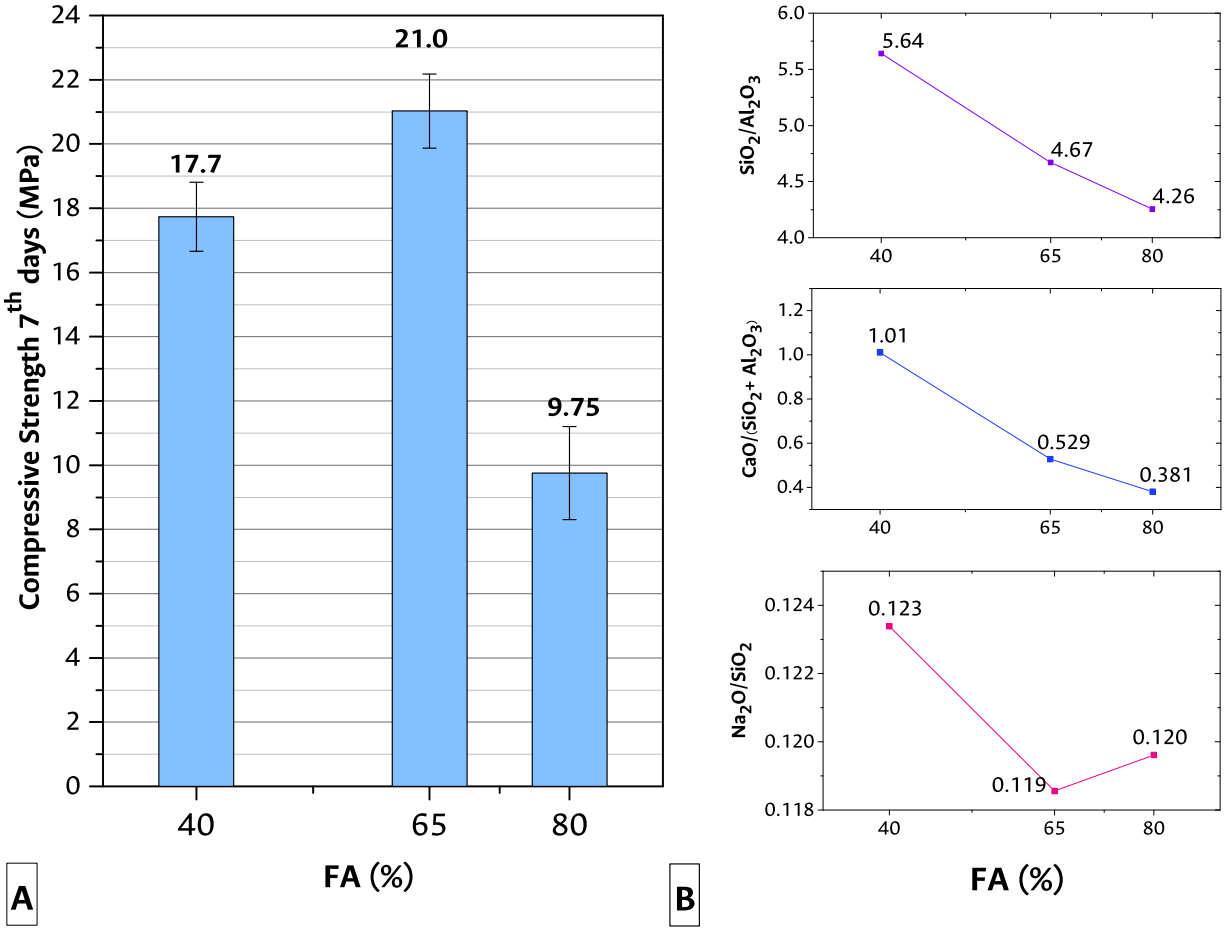

Figure 4-8: FA effect (a) and theorical molar relations (b) for 7 days of curing.

the FA structure, leaving it available to form the hydration products. However, there is a saturation of SiO_2 in the system, as shown by the Na_2O/SiO_2 ratio. In that case, the ionic mobility is reduced, slowing down the formation of the hydration products of a low-calcium AAC cement [76, 77, 85, 115]. On the other hand, the average compressive strength increases significantly while lime quantity is 5 %. This behavior could be explained according to Dombrowski et al.[116] whom assessed the effect of $FA/Ca(OH)_2$ ratio in alkali-activated binders under constant activation conditions; an increased content of $Ca(OH)_2$ in the binder was found to promote the formation of higher amounts of C-S-H type gels in the samples, favoring the evolution of higher mechanical strengths and a more dense binder structure over time.

However, this improvement in mechanical behavior is limited when lime quantity is 10 %. This could been explain taking into account that in a system with significant amounts of lime, the pozzolanic reaction would be the main factor responsible for the compressive strength

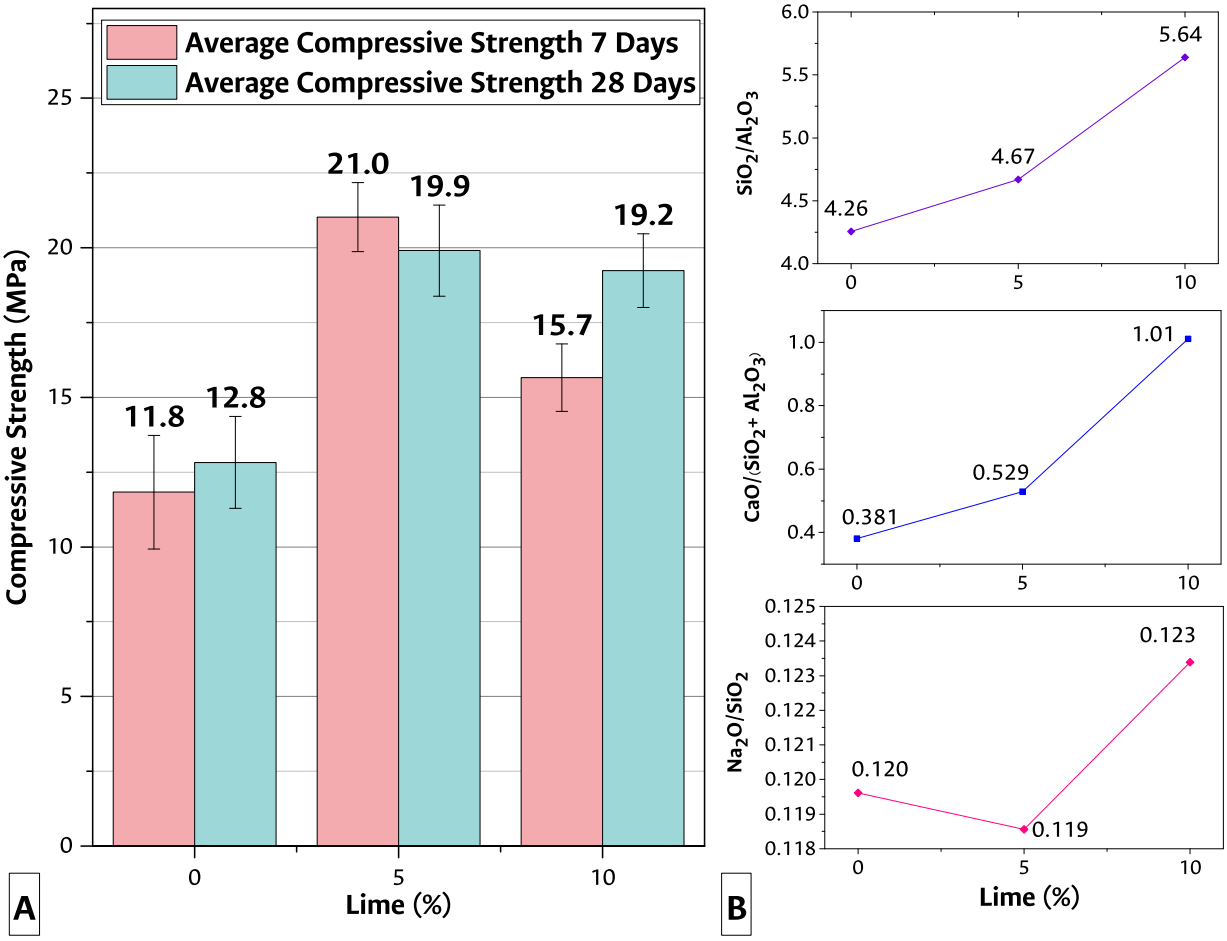

Figure 4-9: Lime effect (a), and theorical molar relations (b) for 7 and 28 days of curing.

obtained. However, if the system is saturated with CH, the limiting reactant of the reaction would be SiO_2 and Al_2O_3 in the system. It is the case at 10 % lime substitution, where the SiO_2/Al_2O_3 ratio is 5.64, the highest evaluated (**Figure 4-9b**); this means that this system contains a lower amount of Al_2O_3, which quickly separates from the precursor structure to form hydration products, which could explain why the strength, although reduced about the central point, does not drop drastically as in the system with 0 % lime. Thus, the compressive strength will also depend on the amount of alkali ions present in the activator solution.

Figure 4-10 shows the effect of the type of lightweight aggregate on the average compressive strength. The horizontal axis shows the treatments evaluated, and the vertical axis shows the average compressive strength for 28^{th} day of curing. This factor also presents a curvature effect at the center point. For aggregate types 1 and 3, there is a reduction in compressive strength. In the case of aggregate type 1, concretes containing 30 % of lightweight polymer waste aggregate, the average compressive strength approach is 14MPa. As reported

by previous research, the damaging effect of stress concentration due to the presence of EPS LWA becomes more pronounced [20, 42, 52, 62, 117, 118, 119]. The presence of EPS, which is an ultra-soft material, redistributes the stresses in the concrete microstructure. On the other hand, bonding with the cementitious matrix is a significant variable in the mechanical properties of composite materials such as concrete. Recycled polymeric aggregates usually bond poorly to the cement paste because they are hydrophobic and their surface is electrically charged. Consequently, neither water nor cement paste is embedded in this LWA. Therefore, material compression fracture tends to occur around the EPS in the void space between the cementitious material and the EPS.

For aggregate type 3, the average compressive strength achieved for the lightweight concretes under study was 18.2MPa, obtaining an average compressive strength 31 % superior to aggregate type 1, which contained a higher EPS percentage, indicating an improvement in bonding with the cementitious matrix as a significant variable in the mechanical properties of composite materials such as concrete [93, 120]. However, the average compressive strength reduction in comparison to aggregate type 2 could be by the lower strength of EC aggregates, resulting in cracking through LWA itself [11, 50, 121, 122].

In the case of aggregate type 2, the highest average compressive strength is obtained with aggregate type 2 (20MPa). This is a polymeric and expanded clays LWA combination. A combined effect of aggregates 1 and 2 is present for this aggregate type. The EC improvement phenomenon of the bonding with the cementitious matrix and the EPS hydrophobic surface redistributes the stresses in the concrete microstructure and causes failure through the paste instead of the EC LWA itself. This failure behavior could explain the compressive strength obtained with aggregate type 2.

Due to the results obtained in the previous section, the Blended 2 mix was selected to manufacture complementary samples that were carried out, according to the proposed methodology. The lightweight aggregate used in these samples was LWA type 2 (15 % EPS and 20 % EC); the binder used was composed of 65 % FA, and 5 % lime were used to prepare blended lightweight concrete, and these samples were cured at 45°C for three days. Then, the blended LWAC was compared to an LWAC using OPC as a cementitious matrix by compressive strength and ITZ microstructure. The results obtained are presented in **Figure 4-11**, where compressive strength and density of the OPC LWAC and blended LWAC for 7^{th} and 28^{th} days of curing is shown.

Moreover, the figure also presents normal-weight concrete compressive strength and density for comparative purposes. The figure shows that the compressive strength between 7^{th} and 28^{th} days of curing for the LWAC evaluated (OPC LWAC and Blended LWAC) increases at a rate of 54 % and 61 %, respectively. Considering that OPC LWAC and Blended LWAC contain the same type of aggregate, in terms of material density, there is a 9 % of reduction as the cementitious matrix is modified. This density reduction can be explained by the blen-

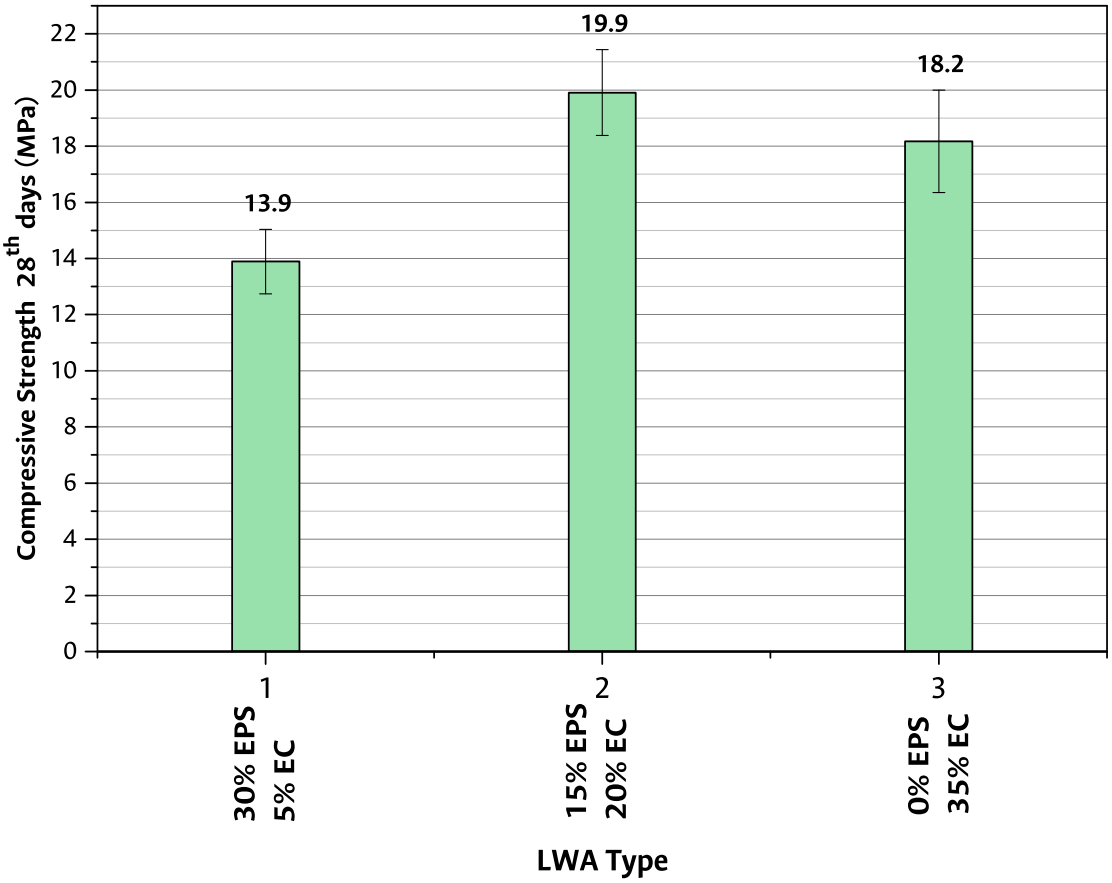

Figure 4-10: LWA Type lineal factor for 28^{th} day of curing.

ded LWAC's materials having densities much lower than those of the OPC LWAC, as was reported in section 4.1.1. While OPC has a 3270kg/m^3 density, FA and Lime have a density of 2160kg/m^3 and 2143kg/m^3, respectively.
A significant reduction in density is observed when comparing the density obtained for the lightweight concretes (OPC LWAC and Blended LWAC) and NWC. According to the data presented in **Figure 4-11**, a reduction of 26 % and 33 % for OPC LWAC and blended LWAC were obtained. As was reported previously in the literature, density reduction affects mechanical performance. Regarding compressive strength, its effects were limited to a decrease of 20 % and 38 % for OPC LWAC and Blended LWAC, respectively.

At this point, it is essential to highlight that Colombian technical regulations classify concrete for structural use with a compressive strength greater than 21MPa at 28^{th} days of curing. Thus, the lightweight concrete obtained in this research project could be used to design a concrete structure. In that case, reducing the cross-section of the elements that make up the structure would be possible. Thus decreasing the dead loads directly related to its own

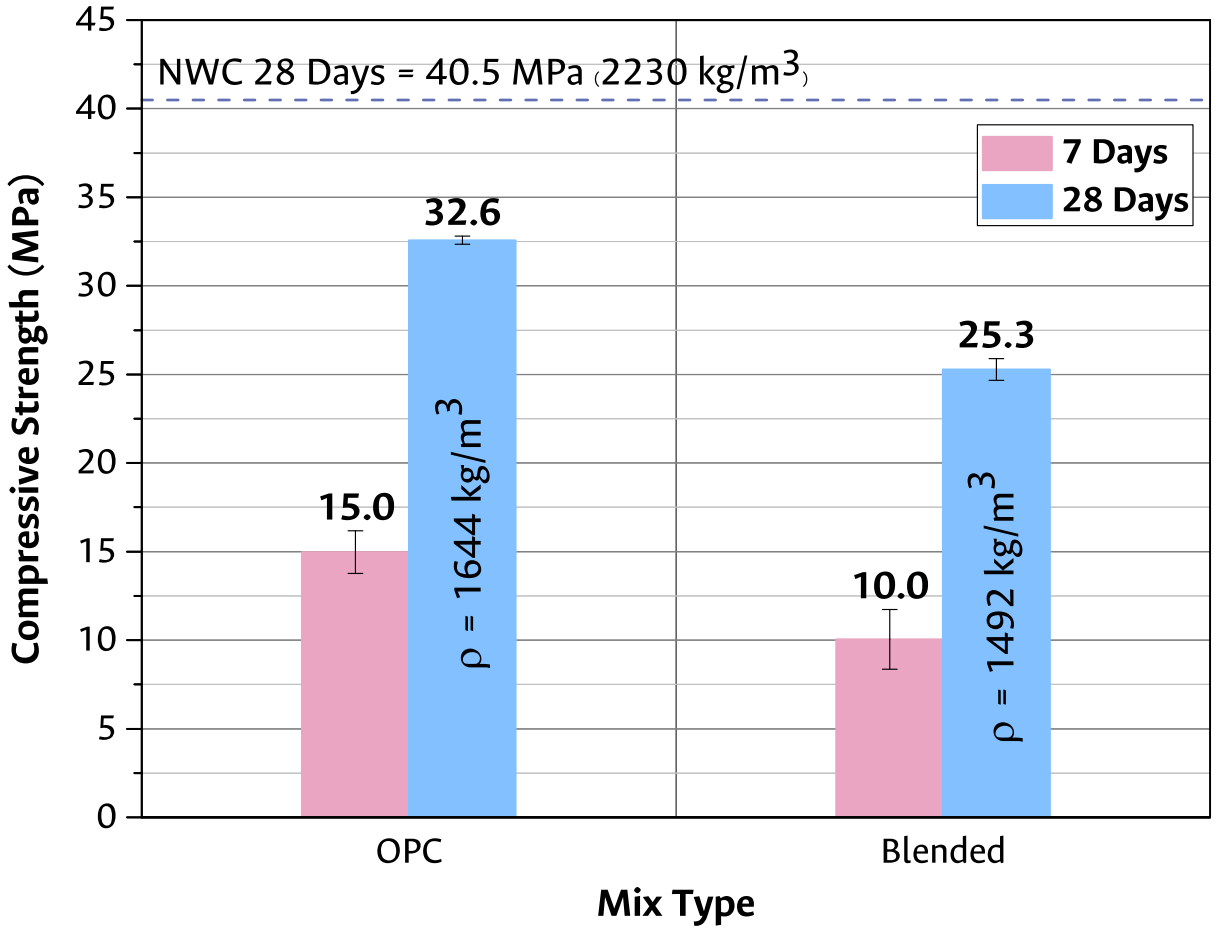

Figure 4-11: Compressive Strength and theoretical density for complementary samples at 7^{th} and 28^{th} Days.

weight. It is finally translated into savings in the total cost of the construction work.

4.2.1. Section Summary

Due to the ANOVA results, the fraction of alkali-activated material (represented in FA and lime replacement percentage) dominates the blended hydration reaction for 7^{th} and 28^{th} days of curing concerning the compressive strength. Besides, the experimental design proposed has a curvature effect in the proportion of 65 % FA and 5 % Lime replacement percentage, where the highest compressive strength was obtained. This indicates that in the proposed lightweight concretes, it is possible to replace up to 70 % of the OPC with alternative cementitious materials (FA and lime), which could reduce the final cost of the material, making it more affordable and with the compressive strength characteristics recommended by the NSR-10 Colombian standard for structural members in a building structural design. Similar results have been previously found in the literature for NWC [78, 88, 114].

In addition, previous research has concluded that an alternative calcium source increases the compressive strength compared with fly ash-based binders because of the coexistence of the main hydration products of both AAC and OPC. In an alkali activation of an aluminosilicate material, such as fly ash type F, sodium aluminosilicate hydrate gel ($N-A-S-H$) is the main hydration product. The reaction becomes more complex when a calcium source is added because the calcium silicate hydrate ($C-S-H$) gels are produced. The $C-S-H$ gel significantly contributes to compressive strength and promotes the setting process [123]. In those cases, the N-A-S-H gel structure has changed to obtain a three-dimensional structure gel called aluminum-substituted calcium silicate ($C-A-S-H$). Therefore, the $N-A-S-H$, $C-(A)-S-H$, and $C-S-H$ type gels can grow simultaneously and coexist in a blended alkali-activated aluminosilicate system [78, 110, 124, 125]. The structural reorganization affects the complementary samples' compressive strength due to the presence of lime and the calcium hydroxide from OPC. The 38 % reduction obtained with the blended LWAC could be due to the incomplete dissolution of the raw materials that make up the blended cement as a function of the amount of activator.

An EPS and EC LWA combination in the LWAC complementary samples leads to the highest average compressive strength. In this type of aggregate, a combined effect is presented. Its incorporation has demonstrated a positive impact, primarily due to EC's ability to bond with the cementitious matrix [11, 50, 121, 122]. and EPS hydrophobic surface [20, 42, 52, 62, 117, 118, 119]. This LWA bonding mechanism effectively redistributes stresses, resulting in failure through the paste rather than the EC LWA.

4.3. Effect of cementitious matrix and LWA replacement on ITZ

Complementary morphological analysis samples were carried out, As described in section 3.2.2. A BSEM micrograph description and porosity quantification results are presented in this section. The threshold values for pore segmentation have also been determined as shown **Table 4-4**. Determining lower and upper threshold values in the histogram pattern is crucial in a quantitative grey scale analysis. Unambiguously, the lower threshold can be set equal to zero. As for the upper threshold, the overflow criterion method was used. Then, 12 successive strips of 5μm width are successfully delineated within images starting at the aggregate surface and up to 60μm away from the aggregate surface as described in section 3.2.4.

Table 4-4: Complementary LWAC samples threshold values for pore segmentation.

Cementitious Matrix	Aggregate Type	Threshold Value
OPC	EPS	$0-50$
100 % OPC	EC	$0-42$
	NWA	$0-36$
Blended	EPS	$0-44$
30 % OPC/ 65 % FA / 5 % Lime	EC	$0-46$
	NWA	$0-44$

Figure 4-12 presents the pores percentage to each strip analyzed from the vicinity of the aggregate used in the complementary samples. In this figure, a lower pores portion around the aggregates in the blended sample can be observed. For the first 20μm of **Figure 4-12a**, a clear decrease in porosity is observed when comparing the blended cementitious matrix with the OPC cement matrix, which could be due to the refinement of the porosity by condensation of the excess SiO_2 contributed by the activator, one of the particular characteristics of ITZ in alkaline activated cementitious materials with the high calcium content [110].

The densification effect typical of LWA, such as expanded clays, is observed in **Figure 4-12b**. Since for the first 15μm around the aggregate and independent of the cementitious matrix, the percentage of pores remains below 10 %, indicating the presence of a well-integrated aggregate-matrix interface. This may be due to calcined clay particles that remain on its surface and have pozzolanic activity [11, 50, 121, 122].
However, the rate of pores in the blended cementitious matrix (**Figure 4-12b**) follows a linear trend with a positive slope. In other words, there is a growth in the pores percentage as the microstructure analysis thickness increases. This behavior could be due to the absorption and subsequent water release from the EC [68], which could affect the molar concentration of the activating solution, negatively affecting the hydration products formed around an EC

within a blended cementitious matrix. In contrast, for the reference sample, this effect seems to favor the microstructure of the material, as the pore percentage tends to remain constant between widths 35μm - 45μm.

In **Figure 4-12c**, a drastic reduction in the percentage of pores in the first 15μm counted from the edge of the EPS lightweight aggregate is observed for the two cementitious matrices. This outcome directly results from the aggregate's hydrophobic nature, which leads to water accumulation around the EPS. Consequently, the porosity decreases as the distance from the aggregate increases, thus substantiating a decline in porosity. This high percentage of pores around the EPS could cause stress redistribution in the LWAC microstructure discussed in the previous section [62]. Furthermore, considering the hydrophobicity of EPS, which will generate activating solution accumulation in the vicinity of the LWA, leading to a greater distance between particles of the cementitious material, limiting the densification of the interfacial transition zone around the aggregate. Therefore, compression cracking of the material tends to occur around the EPS.

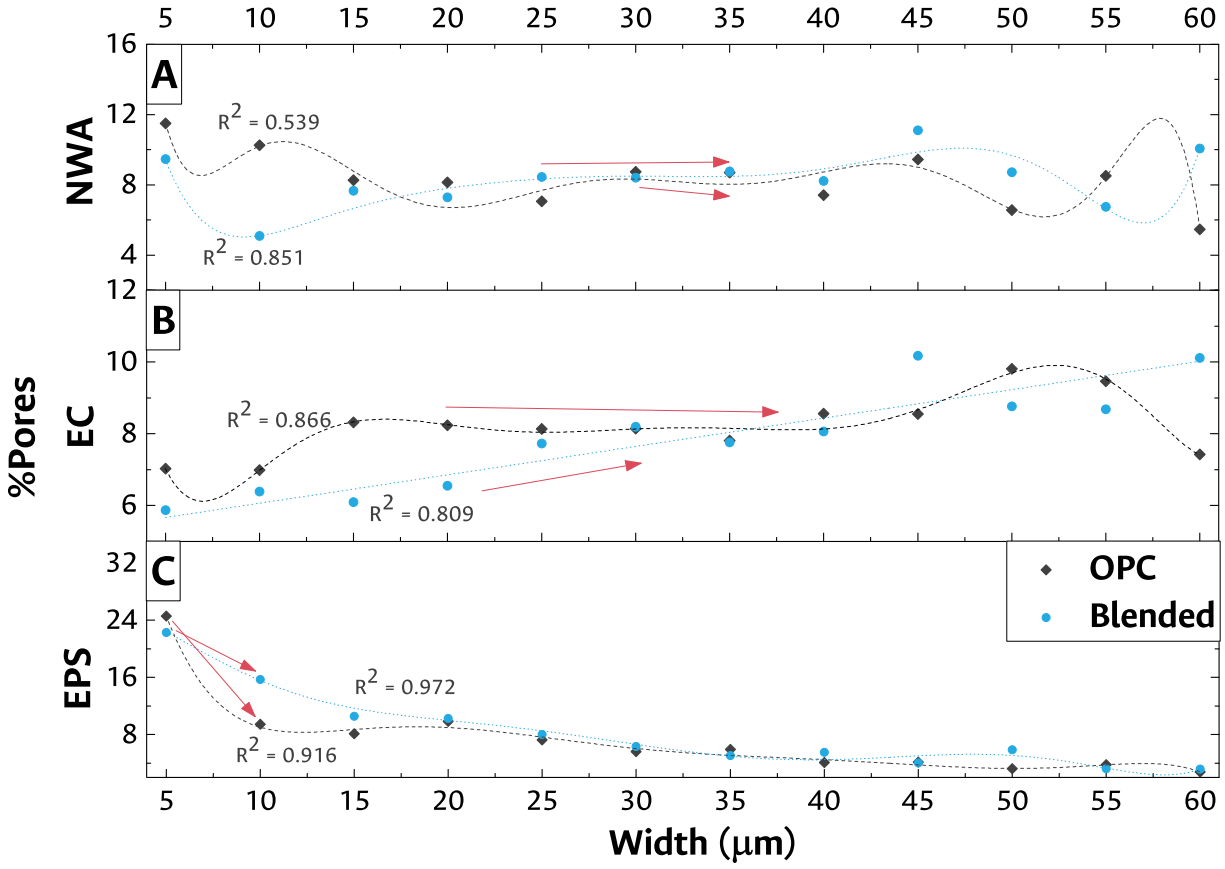

Figure 4-12: Pore percentage for OPC and blended LWAC according to the aggregate type present in the sample. (a) Normal weight aggregate. (b) Expanded Clays lightweight aggregate. (c) Expanded polystyrene lightweight aggregate.

Considering the porosity profile presented in **Figure 4-13a**, the boundary between the ITZ and the cementitious matrix will be the thickness where the percentage of pores tends to a constant. The average thickness of the ITZ for the blended and reference sample is 25μm and 20μm. The pore size distribution for ITZ and bulk paste of the reference and blended LWAC is presented in **Figure 4-13b**, in which it can be observed that the ITZ for both materials has a larger pore size than their respective pastes.

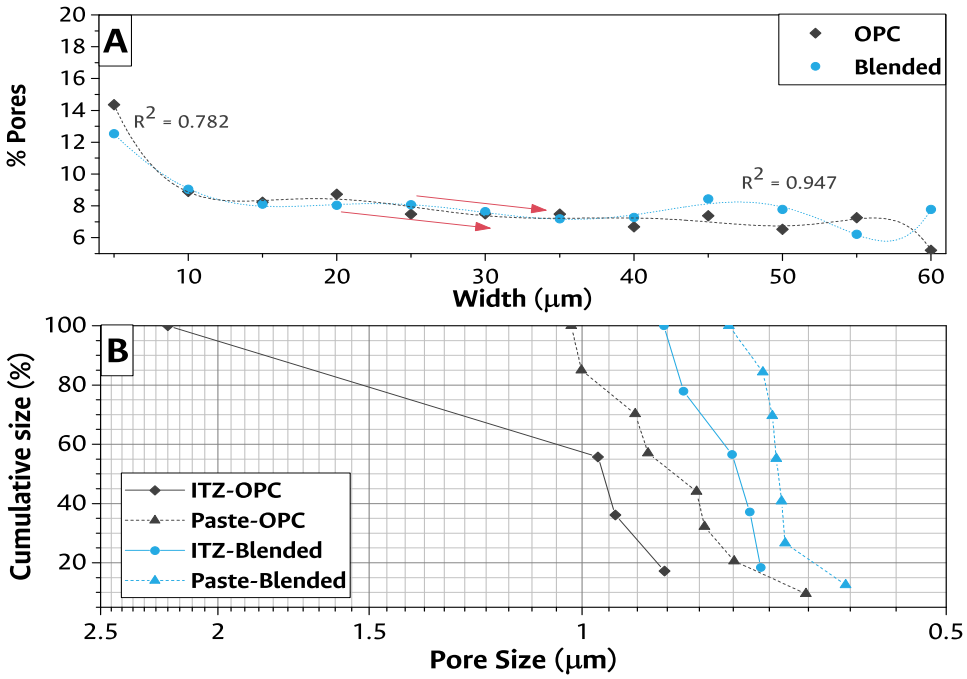

Figure 4-13: (a) Pore percentage and (b) Cumulative pore size for OPC and blended LWAC.

Figure 4-14a-f illustrates the interface between the cementitious matrix and aggregate embedded in the LWAC mixtures. Compared with NWA, EC is porous, as depicted in **Figure 4-14b,e**. Independent of the cementitious matrix, a well-defined interface can be observed between the NWA, which has a relatively smooth surface, and the cementitious matrix, as shown in **Figures 4-14a,d**. In contrast, such a well-defined interface is not observed between the EC and the cementitious matrix due to the irregular and porous surface of the EC. The matrix appears to encapsulate the EC, forming a well-integrated aggregate-matrix interface (**Figure 4-14b,e**).

EPS LWA for the OPC and blended cementitious matrix BSEM Micrographs are shown in **Figure 4-14c,f**. This aggregate type exhibits significant gaps at the interface. This observation is consistent with the weak strength adhesion characteristics of EPS, reported in previous studies [15, 126]. Furthermore, there is a clear difference in the appearance of the blended and OPC matrices when incorporating EPS. While the blended matrix retains a similar appearance for all types of aggregate used, the OPC matrix presents quite marked

differences in the porosity of the ITZ for the LWA EPS (**Figure 4-14c,f**). Comparing cementitious matrices, independently of the type of aggregate, the ITZ for the OPC LWAC sample apparently has more capillary pores and a lower proportion of anhydrous products than the blended LWAC.

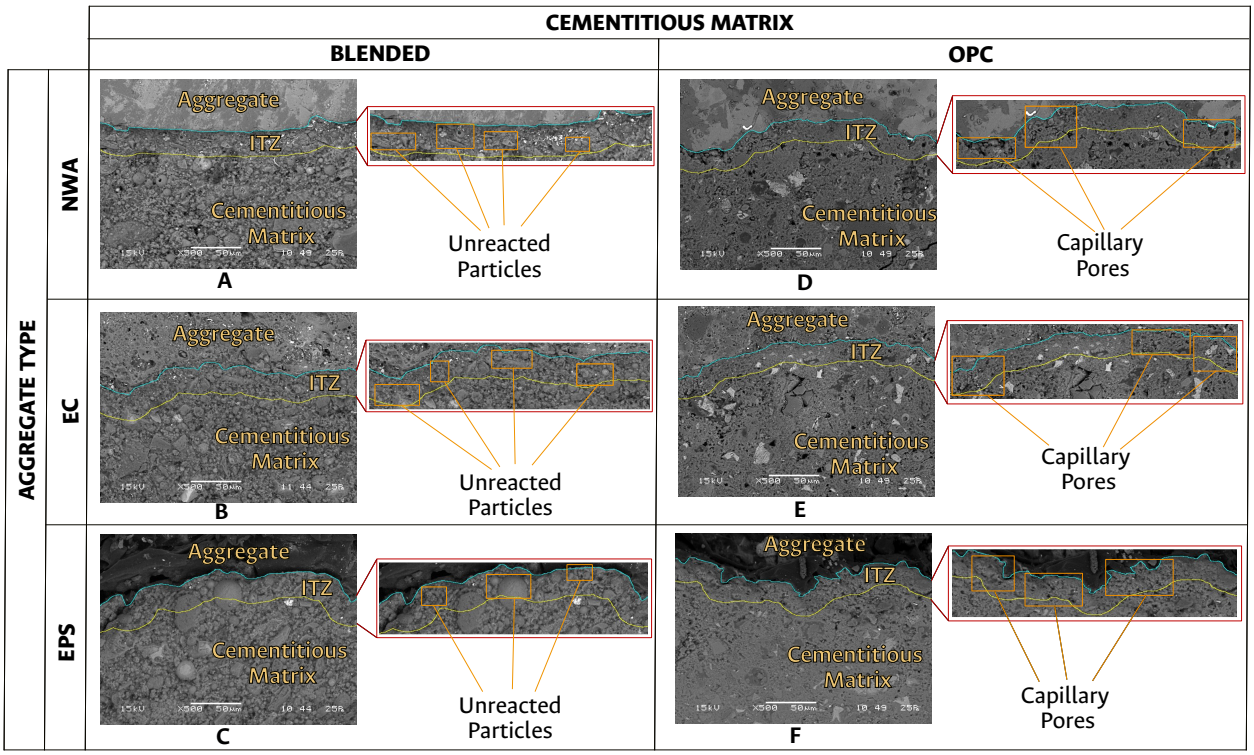

Figure 4-14: BSEM sample micrographs at 500x. According to the cementitious matrix and aggregate type used in LWAC.

In addition, it can be observed that the pore size obtained for the blended sample is lower than that of the reference sample for both ITZ and paste. When reviewing the percentile d50 and d80 presented in **Table 4-5**, it can be observed that the variation in pore size to bulk-paste is between two and four times lower for the blended than the reference sample, indicating a higher densification of the cementitious matrix when using a blended cement.

Table 4-5: Particle size distribution percentiles for the materials under study.

Cementitious Matrix	type	d50	Variation	d80	Variation
OPC	ITZ	0.98	18.1 %	1.53	59.4 %
	Bulk Paste	0.83		0.96	
Blended	ITZ	0.75	8.7 %	0.83	15.3 %
	Bulk Paste	0.69		0.72	

However, this finding does not agree with the mechanical performance obtained in section 4.2. The blended LWAC sample compressive strength was 38 % lower compared to OPC

LWAC. This could be due to the incomplete dissolution of the raw materials that make up the blended cement as a function of the amount of activator. This behavior is observed in the BSEM images, where for blended LWAC, a higher proportion of anhydrous products is observed.

4.3.1. Section Summary

The quantitative image analysis allowed the identification of the approximate thickness of the ITZ in the concretes under study from the porosity calculated every 5μm from the edge of the aggregate. Furthermore, the ITZ for both materials was found to have a larger pore size than their respective pastes, and the pore size obtained for the blended sample is lower than that of the reference sample for both ITZ and bulk-paste. This indicates a higher densification of the cementitious matrix when using blended cement. Thus, quantitatively corroborating what was observed in the BSEM images.

The porosity profile presented for expanded clay (EC) demonstrated the densification effect of EC LWA, limiting the pore percentage in both blended and reference samples and indicating the presence of a well-integrated LWA-matrix interface as was observed in BSEM micrographs. However, for blended LWAC, the pore percentage increases as the ITZ thickness increases. This behavior could be due to the absorption and subsequent water release from the EC [68], negatively affecting the hydration products formed around an EC within a blended cementitious matrix due to the variation in the molar concentration of the activating solution. In contrast, this effect favors the material's microstructure for the reference sample, as the pore percentage tends to remain constant between widths $35\mu\text{m} - 45\mu\text{m}$.

On the other hand, the porosity profile presented for EPS shows a high percentage of pores around the LWA. This phenomenon could cause stress redistribution in the LWAC microstructure discussed in the previous section. Additionally, activating solution accumulation in the vicinity of the LWA leads to a greater distance between particles of the cementitious material, limiting the densification of the interfacial transition zone around the aggregate. Therefore, compression cracking of the material tends to occur around the EPS.

Comparing cementitious matrices, the OPC sample has more capillary pores, and the blended sample apparently has a higher proportion of anhydrous products than the blended matrix (see **Figure 4-14**). This could indicate FA less dissolution rate near the ITZ, promoting failure surfaces and weakening the ITZ.

4.4. Correlation between ITZ and compressive strength performance

The correlation between ITZ pore percentage and compressive strength at 28^{th} days of curing is presented in **Figure 4-15**. From this figure, a directly proportional relationship between compressive strength and pore percentage could be established. This means that the higher the compressive strength, the higher the pores percentage in the ITZ. This result contradicts the report in the literature because, in general, the cementitious matrix porosity directly affects the mechanical behavior of the concrete. However, it is important to note that with a blended cement that uses an AAC and OPC, the mechanical properties mainly depend on the structure and chemical composition of the reaction products, the ions concentration, and the raw material reactivity [127].

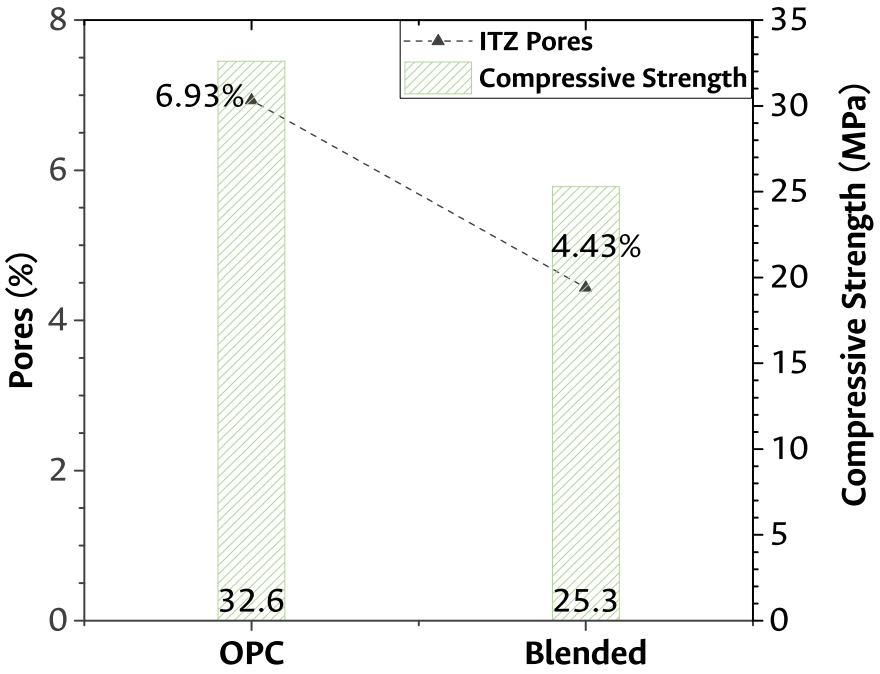

Figure 4-15: Pore percentage and compressive strength for OPC and blended LWAC.

With an increase of Ca and, consequently, a decrease of Al in the AAC system, the dissolution rate could be faster since the formation of $Ca-O-Si$ bonds. As the process advances, because the number of nuclei sites (FA) is reduced, more $C-A-S-H$ gel and less $N-A-S-H$ gel could be formed, which would lead to a lower polymerization degree, a higher cross-linking chain reaction product, and a denser microstructure as was presented on section 4.3. in **Figure 4-13b**.

On the other hand, The Hydroxyl (OH^-), catalyzer (Na^+) content, and curing temperature controls the raw materials dissolution in AAC. A higher amount of free ions, a high amount of

catalyzer, and a temperature of curing that accelerates the FA dissolution reaction improve the formation rate of the $C-(A)-S-H$ gel in the AAC [69, 128]. In the case of blended LWAC studied in this research, the anhydrous product quantities observed could indicate that the activator solution amount or curing of temperature was insufficient. This could indicate FA less dissolution rate near the ITZ, promoting failure surfaces and weakening the ITZ. The previous hypothesis, in addition to the EC and EPS LWA effects discussed in the last section, could explain the behavior of the variables when correlating them.

To compare the reaction rate between OPC and Blended cementitious matrix and corroborate the presence of anhydrous phases in the blended LWAC, pastes were cured at 28^{th} days of curing from complementary samples. They were mineralogically analyzed by XRD and FTIR techniques to identify the hydration products formed and compare the reaction grade for OPC and blended cement that could confirm the difference in compressive strength and morphology observed in complementary samples.

The X-Ray diffractograms for complementary samples at 28^{th} days of curing are reported in **Figure 4-16**. Analysis of the OPC confirmed that the cement hydrated normally. Alite and belite diffraction peaks tend to disappear, indicating $C-S-H$ gel formation, which presents a short-range order to XRD [108, 129]. Secondary hydration products such as Portlandite ($Ca(OH)_2$) and ettringite were also observed in the hydrated cement, as expected. The XRD analysis for blended cement indicates the $C-A-S-H$ and $C-S-H$ prevail under the $N-A-S-H$ gels and the presence of mineral associated with FA were not observed. This behavior was reported previously due to the increment of calcium source in cement [78, 88, 109, 111, 127]. Additionally, as was approached by Hoyos et. al [109, 112] and considering that the CH particle size is, on average, six times smaller than that of FA, CH could form a film on the FA surface during the mixing process of the solids. When the solid part comes in contact with the alkaline activator solution, silicon diffuses firstly to sites with higher sodium presence and in a smaller proportion to sites with calcium presence. In contrast, aluminum diffuses more slowly than silicon, but the presence of calcium stimulates its displacement towards the CH boundary. Because the lattice-forming elements must pass through the CH layer, the first gel formed is the $C-(A)-S-H$ gel around the dissolving FA [87, 112, 109]. The bridging units of the $C-(A)-S-H$ gel act as starting points for forming the $N(C)-A-S-H$ gel which develops between the existing spaces of the gel layers covering the dissolving FA. As the concentration of aluminum increases toward the FA, it is possible that between the unreacted FA and the CH layer, there is a primary gel formed after dissolution, which is rich in aluminum. A Structural reorganization directly affects the compressive strength of the cementitious material [87, 112, 109, 130].
Carbonates, essentially $CaCO_3$, were observed in all samples. The presence of calcium carbonate had a dual explanation. It was present in the anhydrous lime (used for blended cement. **Figure 4-3**) and generated in the hydrated pastes as a result of portlandite carbonation by atmospheric CO_2 [131, 108]. It translated into a decline in the intensity of its diffraction

lines on the 28^{th} day pattern and a rise in the lines associated with carbonates. In addition to carbonating, portlandite may react with the silica and alumina in the FA to generate $C-S-H$ gel-like products (pozzolanic reaction) [131, 108].

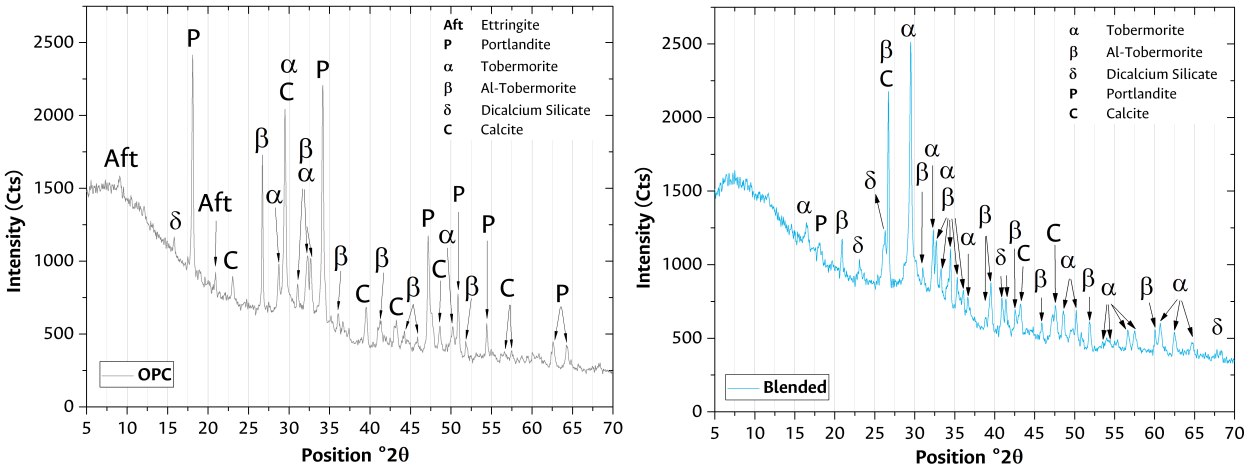

Figure 4-16: Complementary samples X-ray diffraction at 28^{th} Days.

The ampliation of XRD analysis in this study, presented in the **Figure 4-17** is undertaken to elucidate the intricate structural changes occurring within blended cement paste compared to OPC paste. This figure presents a variation in the short-range crystallinity and a slight shift of the maximum value towards higher values of $°2\theta$ of the blended cement paste concerning the OPC cement paste. These changes are related to forming new reaction products, mainly an alkali aluminosilicate gel with a short-range structural order, such as $C-A-S-H$ [82].

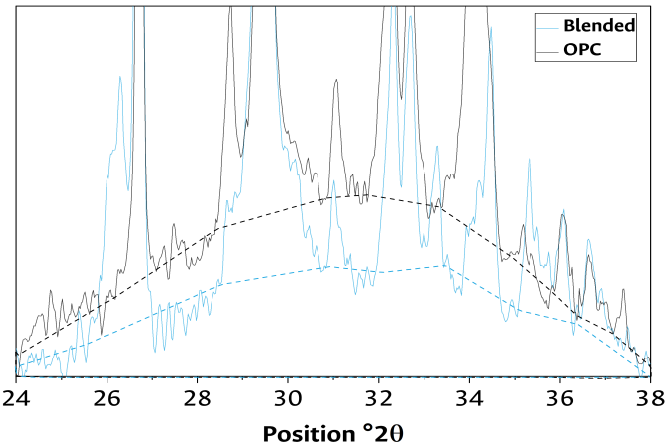

Figure 4-17: Complementary samples short-range crystallinity in X-ray diffraction at 28^{th} Days.

The variation in the intensity of the peak is related to the dissolution of the reactive material of the raw materials that compose the blended cement as a function of the amount

of activator [132] and the displacement with the molecular restructuring for the formation of the cementitious products [133]. Calcium presence modifies the hydrate product's glass structure [134, 135] and contributes to their higher presence. Sodium enrichment by calcium hydroxide (CH) causes the $°2\theta$ position of its major peak to shift towards higher values. A mixture in the presence of CH forms crystalline or semi-crystalline phases of two types, the first of zeolitic character ($Ca_{49.10}Si_{96}Al_{96}O_{384}$) and the second of hydrated calcium silicates ($Ca_{1.5}SiO_{3.5}xH_2O$) [82, 136]. The latter presents a lower range order than that of the fully formed crystal, as seen by comparing the black dashed line with the blue pointed line [137, 138, 139].

To complement mineralogical analysis, the Fourier Transform Infrared (FTIR) Spectroscopy is shown in **Figure 4-18** for complementary samples at 28^{th} days of curing. The broad bands around $3400cm^{-1}$ and, $1640cm^{-1}$ are assigned to the stretching and bending vibrations of ^{-}OH in water, respectively. The band $3641.73cm^{-1}$ is particularly associated with OH^{-} stretching vibrations in $Ca(OH)_2$ [140]. When OPC and blended cement is compared, the bands corresponding to the release of O-H groups present in the hydration products and their reaction with the other mixture elements cause a shift of the wavenumber towards higher values, which could explain the slight difference between the bands $3433cm^{-1}$ and $3439cm^{-1}$ from OPC and blended pastes that shown in **Figure 4-18**. These changes are due to the presence of $Ca-O-H$ units and the capture of mainly silicon and aluminum atoms by hydroxyl groups [141] to form $Si(Al)-O-H$ type structures. These structures and units increase in time due to the formation of new products.

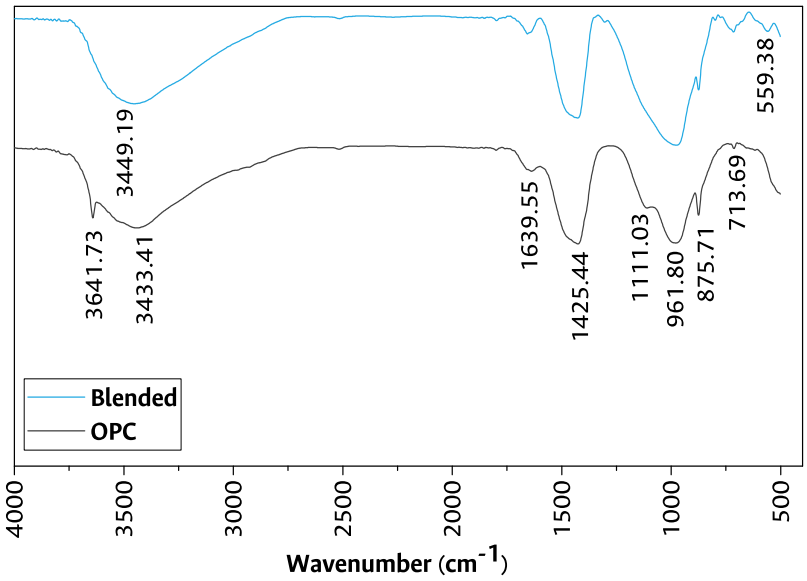

Figure 4-18: Complementary samples Fourier Transform Infrared Spectroscopy at 28^{th} Days.

The bands centered at 1426cm^{-1}, 876cm^{-1} indicate the asymmetric deformation vibration and the CO_3^{2-} wiggle vibration in calcite. The band around 713cm^{-1} represents the main calcite band [140, 111, 142]. this phenomenon is caused due to the presence of calcium carbonate in the CH added to the mixtures and later by the formation of sodium carbonates during the alkaline activation, causing the area to increase [82]. This result is consistent with the XRD findings (**Figure 4-16**).
The main band around 960cm^{-1} associated with asymmetric stretching vibrations of $Si-O$ bonds and bands located at lower wavenumbers assigned to deformation vibrations ($Si-O-Si/Si-O-Al$) [111, 143]. Therefore, these spectra indicate structural features similar to C−A−S−H gel structures.

Particularly, the band around 560cm^{-1}, present in the blended sample, is attributed to the tetrahedral stretching bands of aluminum. The bands in the 690 to 440cm^{-1} range are associated with the bending vibrations generated by the $Si-O-Si/Si-O-Al$ bonds. Some characteristic bands of N−A−S−H gels. A band was likewise observed in the 800cm^{-1} zone, associated with vibrations in the tetrahedra that form the so-called secondary building units (SBU) and fragments of the aluminosilicate network. All this suggests that these gels generally had more intensely polymerized and very likely three-dimensional structures [111]. Bands are present in OPC in 1100 to 1165cm^{-1}, corresponding to SO_4^{-2} in sulfates. The polymerization of SO_4^{-3} and the corresponding vibrations are associated with the presence of ettringite. [142].

FTIR is a powerful analytical technique that provides insights into the molecular composition, structure, and behavior of chemical compounds. However, the FTIR spectra can be complex and challenging to interpret due to overlapping peaks. Deconvoluting curves in FTIR spectroscopy is an essential data processing step aimed at untangling these complexities and extracting valuable information. By isolating individual peaks or bands in the spectrum and characterizing their positions, and intensities, deconvolution facilitates peak identification. This process not only ensures the accuracy and reliability of FTIR data but also holds great significance in a wide range of applications, from basic research to quality control in industries such as materials science.

The main band deconvolution for the blended sample is shown in **Figure 4-19**. It was performed using a Gaussian fit with fit $R^2 = 0.99782$ and OriginLab data analysis software was used. It revealed two key components: one at 976cm^{-1} (a less prominent band at 960cm^{-1}) and the other at 1090cm^{-1}, corresponding to $C-(A)-S-H$ and $N-A-S-H$, respectively. The band at about 976 cm^{-1} represent the $Si-O$ vibrations in the $C-S-H$ groups and the band around 960cm^{-1} is associated with asymmetrical stretching vibrations of $Si-O$ bonds (ν_{as} $Si-O-Si$). This corroborates the presence of such a gel observed in XRD (**Figure 4-16**), indication that the blended sample incorporated calcium into its

structure (as in the conventional $C-S-H$ gel) [111, 140, 142, 143]. The second key band at 1090cm^{-1}, shows the already well recognised substantial shift in position and shape of the ν_{as} $Si-O$ absorption band associated to $N-A-S-H$, gel [110, 144]. In other words, this deconvoluted signal closely resembled the bands of the $C-(A)-S-H$ gel and poorly reached the peaks of the $N-A-S-H$ gel.
This implies that, in this case, the synthesized mixture comprised two fractions, one with a calcium-rich gel and one with a silica-rich gel. According to Guo et al. [140], this signal can be assigned to the stretching vibrations of the Si-O bond in the Q2 tetrahedra. It shifts toward lower frequencies as the Ca/Si ratio increases to values < 1.2, a sign of progressive depolymerization of the silicate chains. The band centered at 874cm^{-1}, indicate the asymmetric wagging vibration of $CO_3{}^{2-}$ in calcite.
It has been previously shown in the literature [82, 109] that the bands corresponding to the $Si-O$ groups are found in a shoulder around the 1170cm^{-1} band. This shoulder tends to disappear as the curing age of the AAC advances, forming compounds resulting in compounds from alkaline activation. In the case of **Figure 4-19**, this shoulder is still present, indicating that a fraction of the FA remains anhydrous at 28^{th} of curing.

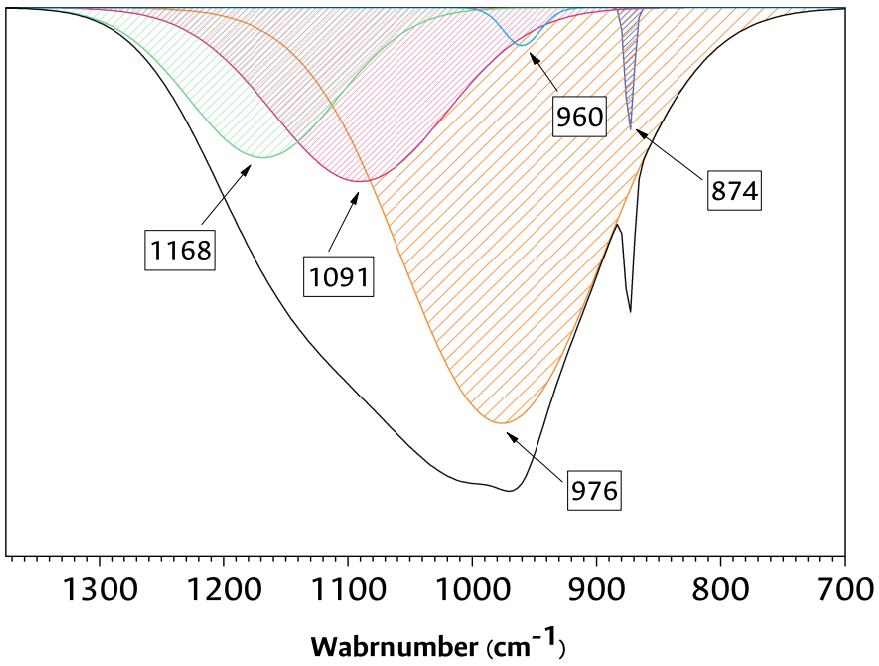

Figure 4-19: Main band deconvolution for the blended sample at 28^{th} Days.

4.4.1. Section Summary

There is a directly proportional relationship between compressive strength and pore percentage (**Figure 4-15**). This result contradicts the report in the literature. It is worth noting

that the mechanical properties of concrete are typically impacted by the porosity of the cementitious matrix. However, when using alternative cement, in this case, a blend between AAC and OPC, the chemical composition, structure of the reaction products, and the concentration of ions influence the mechanical behavior. According to the XRD and FTIR results (**Figure 4-17** and **Figure 4-19**), blended cement has a lower dissolution rate than the reference sample, causing the anhydrous phases presence at 28th days of curing. Consequently, failure surfaces could be produced due to the lower anhydrous phase mechanical strength. This finally caused the weakening of the ITZ.

The deconvoluted FTIR analysis revealed the presence of two key components in the blended sample $C-S-H$ and $C-(A)-S-H$ groups. With a few bands corresponding to the $N-A-S-H$ gel, these results corroborate the results obtained in XRD (**Figure 4-16**). This indicates that the blended sample incorporated CH into its structure (as in the conventional $C-S-H$ gel), leading to a higher cross-linking chain reaction product and a denser microstructure as was obtained in the ITZ pore percentage. Based on the anhydrous product observed, it appears that the amount of activator solution used may have been insufficient. This could result in a slower FA dissolution rate near the ITZ. Such a scenario may lead to the formation of failure surfaces and compromise the strength of the ITZ. Further investigation and adjustments to the activator solution usage may be necessary to ensure optimal outcomes.

5 Chapter 5: Conclusions and Recommendations for Future Research

5.1. Conclusions

The present study investigated the effect on ITZ and compressive strength of replacing cement and aggregates in conventional concrete with AAC and LWA in terms of the porosity and change of phase compositions at the ITZ. Under the conditions and scopes of this experimental study, the main conclusions drawn are summarized below:

5.1.1. General Conclusions

- The generation of hydration products such as $C-A-S-H$, caused the densification of the ITZ. However, the reduction in compressive strength observed in the LWAC manufactured in this project could be explained by the anhydrous phases seen in BSEM images and lower raw material dissolution observed in XRD. The incorporation of EPS and EC in an LWAC also physically impacts compressive strength by redistributing stresses in the microstructure of the LWAC. This is due to the inclusion of brittle and ultra-soft materials that differ from cement paste. Furthermore, the hydrophobicity of EPS causes a lack of adherence of the cementitious material to this LWA. As a result, compression fracture of the material will occur around the EPS in the void space between the cementitious material and the EPS.

- From the proposed DoE, it was possible to determine that the combination with the best mechanical performance corresponds to the central points of the design. That is a blended cementitious matrix comprising 65 % FA, 5 % calcium hydroxide, and just a 30 % of OPC. Additionally, limiting the percentage of EPS substitution to 15 % and replacing the conventional aggregate with 20 % expanded clays. This indicates that in the proposed lightweight concretes, it is possible to replace up to 70 % of the OPC with alternative cementitious materials (fly ash and lime), reducing CO_2 emission.

5.1.2. Specific Conclusions

- The blended lightweight concrete obtained in this research project has a density reduction up to 33 %, with a consequent reduction in compressive strength up to 38 %. Even

so, the mechanical performance obtained is within the compressive strength characteristics recommended by the NSR-10 Colombian standard for structural members in a building and structural design. In that case, reducing the cross-section of the elements that make up the structure would be possible. Thus decreasing the dead loads directly related to its own weight. This could finally be translated into savings in the total cost of the construction work.

- The report results provides a quantitative porosity analysis of EC and EPS in blended and reference samples. The results suggest that EC LWA causes densification in both types of samples, reducing the pore size and demonstrating good integration between LWA and the matrix. However, in blended LWAC, the ITZ thickness is affected by EC's absorption and release of water. This can negatively impact the hydration products formed in the cementitious matrix due to variations in activating solution concentration. In contrast, the reference sample's porosity remains constant, suggesting that its microstructure is unaffected. The porosity analysis of EPS shows a high percentage of pores around the LWA, leading to stress redistribution in the microstructure and compression cracking around the EPS. The accumulation of activating solution around the EPS also limits the densification of the ITZ around this LWA, resulting in an increased distance between particles of the cementitious material.

- The correlation between pore percentage and compressive strength is directly proportional, which contradicts previous literature. Higher capillary porosity typically negatively affects the concrete mechanical behavior, but alternative cement, like a blend between AAC and OPC, is influenced by chemical composition, structure, and ion concentration. The blended cement has a lower dissolution rate as shown by the XRD, produced by the anhydrous phases present, after 28^{th} days of curing. Based on the observed anhydrous product, it appears that the amount of activator solution or the curing temperature used may not have been sufficient, resulting in a slower FA dissolution rate near the ITZ, compromising its strength. Further investigation and adjustments to the activator solution and curing method usage may be necessary for optimal outcomes.

5.2. Recommendations for future research

- According to the results of this project, it is recommended to complete comprehensive knowledge of the behavior of the proposed LWAC, formed with a blended cementitious matrix and recycled polymeric wastes in aggressive environments, and determine their durability properties. It is also recommended to evaluate its acoustic and thermal insulation properties to determine possible coating applications.

- Based on the EC effect when used in blended LWAC, it is recommended to study if its surface is susceptible to alkaline activation by using SH and SS.
- Based on the observed anhydrous product, it is recommended to further investigation and adjustments to activator solution usage for optimal outcomes.
- Currently, the absence of regulations that allow standardization in the production of alternative cementitious materials, such as blended cement and lightweight aggregates from polymeric wastes, limits their application at the industrial level. Therefore, a future line of research recommended from the results obtained in this project is to establish parameters that facilitate the implementation of this material at the industrial scale.
- To quantify the sustainability of the LWAC proposed in this project, it is recommended to perform a life cycle analysis (LCA) and optimize the mix design to reduce the carbon footprint caused by the production of this material.
- Taking into account the importance of predictive models at present, it is recommended as a line of research derived from the results of this research project, to propose a model that can relate the microstructural characteristics of the aggregate, the cementitious matrix, and the ITZ to predict the macrostructural properties such as the compressive strength of the LWACs proposed in this project.

References

[1] ACI Committee 213, "Guide for Structural Lightweight-Aggregate Concrete - (ACI 213R-03)," tech. rep., 2013.

[2] S. Chandra and L. Berntsson, *Lightweight aggregate concrete: Science, Technology, and Applications*. New York: Noyes Publications and William Andrew Publishing, 2002.

[3] J. R. Prestera, D. E. Dixon, and D. A. Crocker, "Standard practice for selecting proportions for structural lightweight concrete (ACI 211.2)," *ACI Materials Journal*, vol. 87, no. 6, pp. 638–651, 1990.

[4] J. Clark, *Structural lightweight aggregate concrete*. Glasgow, UK: Blackie Academic and Profesional, first ed., 1993.

[5] A. Kiliç, C. D. Atiş, E. Yaşar, and F. Özcan, "High-strength lightweight concrete made with scoria aggregate containing mineral admixtures," *Cement and Concrete Research*, vol. 33, no. 10, pp. 1595–1599, 2003.

[6] B. Arisoy and H.-C. Wu, "Material Characteristics of High performance lightweight concrete reinforced with PVA," *Construction and Building Materials*, vol. 22, no. 4, pp. 635–645, 2008.

[7] R. V. Balendran, F. P. Zhou, A. Nadeem, and A. Y. Leung, "Influence of steel fibres on strength and ductility of normal and lightweight high strength concrete," *Building and Environment*, vol. 37, no. 12, pp. 1361–1367, 2002.

[8] D. S. Babu, K. G. Babu, and T. Wee, "Properties of lightweight expanded polystyrene aggregate concretes containing fly ash," *Cement and Concrete Research*, vol. 35, no. 6, pp. 1218–1223, 2005.

[9] J. A. Rossignolo, M. V. Agnesini, and J. A. Morais, "Properties of high-performance LWAC for precast structures with Brazilian lightweight aggregates," *Cement and Concrete Composites*, vol. 25, no. 1, pp. 77–82, 2003.

[10] R. Polat, R. Demirboğa, M. B. Karakoç, and I. Türkmen, "The influence of lightweight aggregate on the physico-mechanical properties of concrete exposed to freeze-thaw cycles," *Cold Regions Science and Technology*, vol. 60, no. 1, pp. 51–56, 2010.

[11] P. Vargas, O. Restrepo-Baena, and J. I. Tobón, "Microstructural analysis of interfacial transition zone (ITZ) and its impact on the compressive strength of lightweight concretes," *Construction and Building Materials*, vol. 137, pp. 381–389, 2017.

[12] I. S. del Bosque, W. Zhu, T. Howind, A. Matías, M. S. de Rojas, and C. Medina, "Properties of interfacial transition zones (itzs) in concrete containing recycled mixed aggregate," *Cement and Concrete Composites*, vol. 81, pp. 25–34, 2017.

[13] M. H. Zhang and V. M. Malhotra, "Characteristics of a thermally activated aluminosilicate pozzolanic material and its use in concrete," *Cement and Concrete Research*, vol. 25, 12 1995.

[14] K. G. Babu and D. S. Babu, "Performance of fly ash concretes containing lightweight EPS aggregates," *Cement and Concrete Composites*, vol. 26, no. 6, pp. 605–611, 2004.

[15] D. González Betancur, E. Andrés, R. García, and H. Gil, "Characterization and Evaluation of Lightweight Fly Ash Concrete Modified with EPS," *International Journal of Civil Engineering and Technology*, vol. 10, no. 8, pp. 288–304, 2019.

[16] Y. Xu, L. Jiang, J. Xu, and Y. Li, "Mechanical properties of expanded polystyrene lightweight aggregate concrete and brick," *Construction and Building Materials*, vol. 27, no. 1, pp. 32–38, 2012.

[17] A. Habib, U. Yildirm, and O. Eren, "Mechanical and dynamic properties of high strength concrete with well graded coarse and fine tire rubber," *Construction and Building Materials*, vol. 246, p. 118502, 2020.

[18] E. del Rey Castillo, N. Almesfer, O. Saggi, and J. M. Ingham, "Light-weight concrete with artificial aggregate manufactured from plastic waste," *Construction and Building Materials*, vol. 265, p. 120199, 2020.

[19] I. Almeshal, B. A. Tayeh, R. Alyousef, H. Alabduljabbar, and A. M. Mohamed, "Eco-friendly concrete containing recycled plastic as partial replacement for sand," *Journal of Materials Research and Technology*, vol. 9, no. 3, pp. 4631–4643, 2020.

[20] F. Aslani, A. Deghani, and Z. Asif, "Development of lightweight rubberized geopolymer concrete by using polystyrene and recycled crumb-rubber aggregates," *Journal of Materials in Civil Engineering*, vol. 32, no. 2, p. 04019345, 2020.

[21] W. Zhai, J. Ding, X. An, and Z. Wang, "An optimization model of sand and gravel mining quantity considering healthy ecosystem in yangtze river, china," *Journal of Cleaner Production*, vol. 242, p. 118385, 2020.

[22] S. A. Miller and F. C. Moore, "Climate and health damages from global concrete production," *Nature Climate Change*, vol. 10, no. 5, pp. 439–443, 2020.

[23] C. Shi, A. F. Jiménez, and A. Palomo, "New cements for the 21st century: The pursuit of an alternative to Portland cement," *Cement and Concrete Research*, vol. 41, no. 7, pp. 750–763, 2011.

[24] J. S. Van Deventer, J. L. Provis, and P. Duxson, "Technical and commercial progress in the adoption of geopolymer cement," *Minerals Engineering*, vol. 29, pp. 89–104, 2012.

[25] L. N. Assi, K. Carter, E. Deaver, and P. Ziehl, "Review of availability of source materials for geopolymer/sustainable concrete," *Journal of Cleaner Production*, vol. 263, p. 121477, 2020.

[26] C. Sharma and K. Qanungo, "An overview: Recycling of expanded polystyrene foam," *AIP Conference Proceedings*, vol. 2535, 05 2023.

[27] T. Y. Suman, P. P. Jia, W. G. Li, M. Junaid, G. Y. Xin, Y. Wang, and D. S. Pei, "Acute and chronic effects of polystyrene microplastics on brine shrimp: First evidence highlighting the molecular mechanism through transcriptome analysis," *Journal of Hazardous Materials*, vol. 400, no. June, p. 123220, 2020.

[28] C. Xu, B. Zhang, C. Gu, C. Shen, S. Yin, M. Aamir, and F. Li, "Are we underestimating the sources of microplastic pollution in terrestrial environment?," *Journal of Hazardous Materials*, vol. 400, no. February, p. 123228, 2020.

[29] A. Zaragoza-Benzal and D. Ferrández and E. Atanes-Sánchez and C. Morón, "New lightened plaster material with dissolved recycled expanded polystyrene and end-of-life tyres fibres for building prefabricated industry," *Case Studies in Construction Materials*, vol. 18, p. e02178, 2023.

[30] Z. Li and X. Shi, "Graphene oxide modified, clinker-free cementitious paste with principally alkali-activated fly ash," *Fuel*, vol. 269, no. February, p. 117418, 2020.

[31] M. Záleská, Z. Pavlík, D. Čítek, O. Jankovský, and M. Pavlíková, "Eco-friendly concrete with scrap-tyre-rubber-based aggregate Properties and thermal stability," *Construction and Building Materials*, vol. 225, pp. 709–722, nov 2019.

[32] N. Saikia and J. D. Brito, "Use of plastic waste as aggregate in cement mortar and concrete preparation: A review," *Construction and Building Materials*, vol. 34, pp. 385–401, 2012.

[33] R. Sharma and P. P. Bansal, "Use of different forms of waste plastic in concrete − A review," *Journal of Cleaner Production*, vol. 112, pp. 473–482, 2016.

[34] J. Xie, J. Wang, B. Zhang, C. Fang, and L. Li, "Physicochemical properties of alkali activated GGBS and fly ash geopolymeric recycled concrete," *Construction and Building Materials*, vol. 204, pp. 384–398, 2019.

[35] J. Davidovits, "False values on CO_2 emission for Geopolymer Cement/Concrete published in scientific papers," tech. rep., 2015.

[36] Y. Guo, L. Luo, T. Liu, L. Hao, Y. Li, P. Liu, and T. Zhu, "A review of low-carbon technologies and projects for the global cement industry," *Journal of Environmental Sciences*, vol. 136, pp. 682–697, 2024.

[37] M. G. Plaza, S. Martínez, and F. Rubiera, "CO_2 Capture, Use, and Storage in the Cement Industry: State of the Art and Expectations," *Energies*, vol. 13, no. 21, 2020.

[38] J. Davidovits, *Geopolymer Chemistry and Applications*. Geopolymer Institute, 2nd ed., 2008.

[39] J. S. Van Deventer, J. L. Provis, P. Duxson, and D. G. Brice, "Chemical research and climate change as drivers in the commercial adoption of alkali activated materials," *Waste and Biomass Valorization*, vol. 1, no. 1, pp. 145–155, 2010.

[40] P. Monteiro, J. Maso, and J. Ollivier, "The aggregate-mortar interface," *Cement and Concrete Research*, vol. 15, pp. 953–958, nov 1985.

[41] "ASTM C33/C33M-18. Standard Specification for Concrete Aggregates," 2018.

[42] D. S. Babu, K. Ganesh Babu, and W. Tiong-Huan, "Effect of polystyrene aggregate size on strength and moisture migration characteristics of lightweight concrete," *Cement and Concrete Composites*, vol. 28, no. 6, pp. 520–527, 2006.

[43] M.-H. Zhang and O. E. Gjørv, "Microstructure of the interfacial zone between lightweight aggregate and cement paste," *Cement and Concrete Research*, vol. 20, pp. 610–618, jul 1990.

[44] P. Vargas Samboni, "Evaluación de la influencia de propiedades físicas y morfolígicas de agregados livianos, en la microestructura de la Zona de Transición Interfacial (ITZ), en concretos," Master's thesis, Universidad Nacional de Colombia, 2016.

[45] M.-H. Zhang and O. E. Gjørv, "Characteristics of Lightweight Aggregates for High-Strength Concrete," *ACI Materials Journal*, vol. 88, no. 2, 1991.

[46] Z. Li, *Advanced Concrete Technology*. John Wiley & Sons, Ltd, 2011.

[47] V. Ferrándiz-Mas and E. García-Alcocel, "Durability of expanded polystyrene mortars," *Construction and Building Materials*, vol. 46, pp. 175–182, 2013.

[48] A. L. Brooks, H. Zhou, and D. Hanna, "Comparative study of the mechanical and thermal properties of lightweight cementitious composites," *Construction and Building Materials*, vol. 159, pp. 316–328, 2018.

[49] A. Hanif, Z. Lu, Y. Cheng, S. Diao, and Z. Li, "Effects of Different Lightweight Functional Fillers for Use in Cementitious Composites," *International Journal of Concrete Structures and Materials*, vol. 11, no. 1, pp. 99–113, 2017.

[50] C. Muñoz-Ruiperez, A. Rodríguez, S. Gutiérrez-González, and V. Calderón, "Lightweight masonry mortars made with expanded clay and recycled aggregates," *Construction and Building Materials*, vol. 118, pp. 139–145, 2016.

[51] O. Sengul, S. Azizi, F. Karaosmanoglu, and M. A. Tasdemir, "Effect of expanded perlite on the mechanical properties and thermal conductivity of lightweight concrete," *Energy and Buildings*, vol. 43, no. 2, pp. 671–676, 2011.

[52] A. F. Angelin, R. C. Cecche Lintz, W. R. Osório, and L. A. Gachet, "Evaluation of efficiency factor of a self-compacting lightweight concrete with rubber and expanded clay contents," *Construction and Building Materials*, vol. 257, p. 119573, 2020.

[53] M. Lanzón, V. Cnudde, T. De Kock, and J. Dewanckele, "Microstructural examination and potential application of rendering mortars made of tire rubber and expanded polystyrene wastes," *Construction and Building Materials*, vol. 94, pp. 817–825, 2015.

[54] J. N. Asaad and S. Y. Tawfik, "Polymeric composites based on polystyrene and cement dust wastes," *Materials and Design*, vol. 32, no. 10, pp. 5113–5119, 2011.

[55] S. Akçaözoğlu, C. D. Atiş, and K. Akçaözoğlu, "An investigation on the use of shredded waste PET bottles as aggregate in lightweight concrete," *Waste Management*, vol. 30, no. 2, pp. 285–290, 2010.

[56] Mehta, P. Kumar and Monteiro, Paulo J.M., *Concrete: Microstructure, Properties, and Materials*. New York: McGraw-Hill Education, 3rd ed., 2006.

[57] L. Gu and T. Ozbakkaloglu, "Use of recycled plastics in concrete: A critical review," *Waste Management*, vol. 51, pp. 19–42, 2016.

[58] K. Miled, K. Sab, and R. Le Roy, "Particle size effect on EPS lightweight concrete compressive strength: Experimental investigation and modelling," *Mechanics of Materials*, vol. 39, no. 3, pp. 222–240, 2007.

[59] F. Pacheco-Torgal, S. Jalali, J. A. Labrincha, and V. M. John, eds., *Eco-Efficient Concrete*. Woodhead Publishing, 2013.

[60] B. Chen and C. Fang, "Mechanical properties of EPS lightweight concrete," in *Proceedings of the Institution of Civil Engineers - Construction Materials*, vol. 164, pp. 173–180, 2011.

[61] X. Li, T.-C. Ling, and K. Hung Mo, "Functions and impacts of plastic/rubber wastes as eco-friendly aggregate in concrete – a review," *Construction and Building Materials*, vol. 240, p. 117869, 2020.

[62] M. Bakhshi and S. Shahbeyk, "Experimental and microstructural study of the compressive strength of concrete samples containing low volumes of expanded polystyrene beads," *Structural Concrete*, vol. 20, no. 4, pp. 1379–1390, 2019.

[63] M. Fathi, A. Yousefipour, and E. H. Farokhy, "Mechanical and physical properties of expanded polystyrene structural concretes containing micro-silica and nano-silica," *Construction and Building Materials*, vol. 136, pp. 590–597, 2017.

[64] M. Maaroufi, K. Abahri, C. E. Hachem, and R. Belarbi, "Characterization of EPS lightweight concrete microstructure by X-ray tomography with consideration of thermal variations," *Construction and Building Materials*, vol. 178, pp. 339–348, 2018.

[65] D. Bouvard, J. M. Chaix, R. Dendievel, A. Fazekas, J. M. Létang, G. Peix, and D. Quenard, "Characterization and simulation of microstructure and properties of EPS lightweight concrete," *Cement and Concrete Research*, vol. 37, no. 12, pp. 1666–1673, 2007.

[66] C. Albano, N. Camacho, M. Hernández, A. Matheus, and A. Gutiérrez, "Influence of content and particle size of waste pet bottles on concrete behavior at different w/c ratios," *Waste Management*, vol. 29, no. 10, pp. 2707–2716, 2009.

[67] R. Le Roy, E. Parant, and C. Boulay, "Taking into account the inclusions' size in lightweight concrete compressive strength prediction," *Cement and Concrete Research*, vol. 35, no. 4, pp. 770–775, 2005.

[68] P. Vargas, N. A. Marín, and J. I. Tobón, "Performance and Microstructural Analysis of Lightweight Concrete Blended with Nanosilica under Sulfate Attack," *Advances in Civil Engineering*, vol. 2018, Article ID 2715474, pp. 1–11, 2018.

[69] P. Zhang, K. Wang, Q. Li, J. Wang, and Y. Ling, "Fabrication and engineering properties of concretes based on geopolymers/alkali-activated binders - A review," *Journal of Cleaner Production*, vol. 258, pp. 1–22, 2020.

[70] R. San Nicolas and J. L. Provis, "The interfacial transition zone in alkali-activated slag mortars," *Frontiers in Materials*, vol. 2, no. 70, pp. 1–11, 2015.

[71] A. Fernández-Jiménez and A. Palomo, "Characterisation of fly ashes. Potential reactivity as alkaline cements," *Fuel*, vol. 82, no. 18, pp. 2259–2265, 2003.

[72] G. Fang and M. Zhang, "The evolution of interfacial transition zone in alkali-activated fly ash-slag concrete," *Cement and Concrete Research*, vol. 129, pp. 1–21, 2020.

[73] W. Lee and J. van Deventer, "The interface between natural siliceous aggregates and geopolymers," *Cement and Concrete Research*, vol. 34, no. 2, pp. 195–206, 2004.

[74] S. M.A. and O. G.J., "Slag/fly ash cements," tech. rep., U.S. Department of Energy - Office of Scientific and Technical Information, Nov 1977.

[75] F. Puertas, S. Martínez-Ramírez, S. Alonso, and T. Vázquez, "Alkali-activated fly ash/slag cements: Strength behaviour and hydration products," *Cement and Concrete Research*, vol. 30, no. 10, pp. 1625–1632, 2000.

[76] N. Lee and H. Lee, "Reactivity and reaction products of alkali-activated, fly ash/slag paste," *Construction and Building Materials*, vol. 81, pp. 303–312, 2015.

[77] J. Provis and J. van Deventer, *Alkali Activated Materials: State-of-the-Art Report, RILEM TC 224-AAM*. RILEM State-of-the-Art Reports, Springer Netherlands, 2013.

[78] I. García-Lodeiro, A. Fernández-Jiménez, and A. Palomo, "Variation in hybrid cements over time. Alkaline activation of fly ash-portland cement blends," *Cement and Concrete Research*, vol. 52, pp. 112–122, 2013.

[79] P. Posi, C. Teerachanwit, C. Tanutong, S. Limkamoltip, S. Lertnimoolchai, V. Sata, and P. Chindaprasirt, "Lightweight geopolymer concrete containing aggregate from recycle lightweight block," *Materials and Design*, vol. 52, pp. 580–586, 2013.

[80] D. M. Huiskes, A. Keulen, Q. L. Yu, and H. J. Brouwers, "Design and performance evaluation of ultra-lightweight geopolymer concrete," *Materials and Design*, vol. 89, pp. 516–526, 2016.

[81] A. Wongsa, Y. Zaetang, V. Sata, and P. Chindaprasirt, "Properties of lightweight fly ash geopolymer concrete containing bottom ash as aggregates," *Construction and Building Materials*, vol. 111, pp. 637–643, 2016.

[82] A. A. Hoyos-Montilla, F. Puertas, and J. I. Tobón, "Microcalorimetric study of the effect of calcium hydroxide and temperature on the alkaline activation of coal fly ash," *Journal of Thermal Analysis and Calorimetry*, vol. 131, no. 3, pp. 2395–2410, 2018.

[83] C. Shi, P. V. Krivenko, and D. Roy, *Alkali-Activated Cements and Concretes*. New York: CRC Press, 2003.

[84] F. Pacheco-Torgal, J. Labrincha, C. Leonelli, A. Palomo, and Chindaprasirt P., *Handbook of Alkali-Activated Cements, Mortars and Concretes*. Woodhead Publishing, 2015.

[85] J. L. P. van Deventer and J. S.J., *Geopolymers: Structure, processing, propierties and industrial applications*. Cambridge: Woodhead Publishing Limited, 2009.

[86] A. Mehta and R. Siddique, "Properties of low-calcium fly ash based geopolymer concrete incorporating OPC as partial replacement of fly ash," *Construction and Building Materials*, vol. 150, pp. 792–807, 2017.

[87] A. A. Hoyos-Montilla, F. Puertas, and J. I. Tobón, "Study of the reaction stages of alkali-activated cementitious materials using microcalorimetry," *Advances in Cement Research*, vol. 33, no. 1, pp. 1–13, 2021.

[88] J. M. Mejía, E. Rodríguez, R. Mejía De Gutiérrez, and N. Gallego, "Preparation and characterization of a hybrid alkaline binder based on a fly ash with no commercial value," *Journal of Cleaner Production*, vol. 104, pp. 346–352, 2015.

[89] I. Garcia-Lodeiro, V. Carcelen-Taboada, A. Fernández-Jiménez, and A. Palomo, "Manufacture of hybrid cements with fly ash and bottom ash from a municipal solid waste incinerator," *Construction and Building Materials*, vol. 105, pp. 218–226, 2016.

[90] I. Garcia Lodeiro, N. Cristelo, A. Palomo, and A. Fernández-Jiménez, "Use of industrial by-products as alkaline cement activators," *Construction and Building Materials*, vol. 253, p. 119000, 2020.

[91] E. Acevedo-Martinez, L. Gomez-Zamorano, and J. Escalante-Garcia, "Portland cement-blast furnace slag mortars activated using waterglass: - Part 1: Effect of slag replacement and alkali concentration," *Construction and Building Materials*, vol. 37, pp. 462–469, 2012.

[92] R. Madandoust, M. M. Ranjbar, and S. Yasin Mousavi, "An investigation on the fresh properties of self-compacted lightweight concrete containing expanded polystyrene," *Construction and Building Materials*, vol. 25, no. 9, pp. 3721–3731, 2011.

[93] A. M. Rashad, "Lightweight expanded clay aggregate as a building material – An overview," *Construction and Building Materials*, vol. 170, pp. 757–775, 2018.

[94] K. Scrivener, R. Snellings, and B. Lothenbach, *A Practical Guide to Microstructural Analysis of Cementitious Materials*. CRC Press, 2018.

[95] K. L. Scrivener, V. M. John, and E. M. Gartner, "Eco-efficient cements: Potential economically viable solutions for a low-CO_2 cement-based materials industry," *Cement and Concrete Research*, vol. 114, no. December, pp. 2–26, 2018.

[96] P. Pavithra, M. Srinivasula Reddy, P. Dinakar, B. Hanumantha Rao, B. K. Satpathy, and A. N. Mohanty, "A mix design procedure for geopolymer concrete with fly ash," *Journal of Cleaner Production*, vol. 133, pp. 117–125, 2016.

[97] J. Ibáñez, O. Font, N. Moreno, J. Elvira, S. Alvarez, and X. Querol, "Quantitative rietveld analysis of the crystalline and amorphous phases in coal fly ashes," *Fuel*, vol. 105, pp. 314–317, 2013.

[98] Y. Gao, G. De Schutter, G. Ye, H. Huang, Z. Tan, and K. Wu, "Porosity characterization of ITZ in cementitious composites: Concentric expansion and overflow criterion," *Construction and Building Materials*, vol. 38, pp. 1051–1057, 2013.

[99] S. Diamond, "Considerations in image analysis as applied to investigations of the ITZ in concrete," *Cement and Concrete Composites*, vol. 23, no. 2-3, pp. 171–178, 2001.

[100] Y. Gao, G. De Schutter, G. Ye, Z. Tan, and K. Wu, "The ITZ microstructure, thickness and porosity in blended cementitious composite: Effects of curing age, water to binder ratio and aggregate content," *Composites Part B: Engineering*, vol. 60, pp. 1–13, 2014.

[101] H. S. Wong, M. K. Head, and N. R. Buenfeld, "Pore segmentation of cement-based materials from backscattered electron images," *Cement and Concrete Research*, vol. 36, no. 6, pp. 1083–1090, 2006.

[102] H. Wong and N. Buenfeld, "Patch microstructure in cement-based materials: Fact or artefact?," *Cement and Concrete Research*, vol. 36, no. 5, pp. 990–997, 2006.

[103] S. Diamond and M. E. Leeman, "Pore size distributions in hardened cement paste by sem image analysis," in *MRS Online Proceedings Library (OPL)*, vol. 370, p. 217, Cambridge University Press, 1994.

[104] K. Komnitsas, D. Zaharaki, and V. Perdikatsis, "Effect of synthesis parameters on the compressive strength of low-calcium ferronickel slag inorganic polymers," *Journal of Hazardous Materials*, vol. 161, no. 2, pp. 760–768, 2009.

[105] W. A. Bautista-Ruiz, M. Díaz-Lagos, and S. A. Martínez-Ovalle, "Caracterización de las cenizas volantes de una planta termoeléctrica para su posible uso como aditivo en la fabricación de cemento," *Revista de Investigación, Desarrollo e Innovación*, vol. 8, pp. 135–146, dic. 2017.

[106] D. Gómez-Cano, J. C. Ochoa-Botero, R. B. Correa, and Y. P. Arias, "Mechanical Behavior of Recycled Mortars Manufactured from Moisture Correction Using the Halogen Light Thermogravimetric Balance as an Alternative to the Traditional ASTM C 128 Method," *International Journal of Structural and Construction Engineering*, vol. 16, no. 6, pp. 164 – 168, 2022.

[107] A. Elsharief, M. D. Cohen, and J. Olek, "Influence of lightweight aggregate on the microstructure and durability of mortar," *Cement and Concrete Research*, vol. 35, no. 7, pp. 1368–1376, 2005.

[108] H. F. W. Taylor, *Cement Chemistry*. London: Academic Press, 1990.

[109] A. A. Hoyos-Montilla, J. I. Tobón, and F. Puertas, "Role of calcium hydroxide in the alkaline activation of coal fly ash," *Cement and Concrete Composites*, vol. 137, p. 104925, 2023.

[110] I. García-Lodeiro, A. Palomo, A. Fernández-Jiménez, and D. E. MacPhee, "Compatibility studies between N-A-S-H and C-A-S-H gels. Study in the ternary diagram $Na_2O - CaO - Al_2O_3 - SiO_2 - H_2O$," *Cement and Concrete Research*, vol. 41, no. 9, pp. 923–931, 2011.

[111] I. García-Lodeiro, A. Fernández-Jiménez, M. T. Blanco, and A. Palomo, "FTIR study of the sol−gel synthesis of cementitious gels: C−S−H and N−A−S−H," *Journal of Sol-Gel Science and Technology*, vol. 45, no. 1, pp. 63–72, 2008.

[112] A. A. Hoyos-Montilla, F. Puertas, J. Molina Mosquera, and J. I. Tobón, "Infrared spectra experimental analyses on alkali-activated fly ash-based binders," *Spectrochimica Acta Part A: Molecular and Biomolecular Spectroscopy*, vol. 269, p. 120698, 2022.

[113] L. Gomez-Zamorano, M. Balonis, B. Erdemli, N. Neithalath, and G. Sant, "C-(N)-S-H and N-A-S-H gels: Compositions and solubility data at 25 °C and 50 °C," *Journal of the American Ceramic Society*, vol. 100, no. 6, pp. 2700–2711, 2017.

[114] I. García-Lodeiro, A. Fernández-Jiménez, A. Palomo, and D. E. MacPhee, "Effect of calcium additions on N-A-S-H cementitious gels," *Journal of the American Ceramic Society*, vol. 93, no. 7, pp. 1934–1940, 2010.

[115] S. Kumar and R. Kumar, "Mechanical activation of fly ash: Effect on reaction, structure and properties of resulting geopolymer," *Ceramics International*, vol. 37, pp. 533–541, 2011.

[116] K. Dombrowski, A. Buchwald, and M. Weil, "The influence of calcium content on the structure and thermal performance of fly ash based geopolymers," *Journal of Materials Science*, vol. 42, no. 9, pp. 3033–3043, 2007.

[117] A. F. Angelin, F. M. Da Silva, L. A. Barbosa, R. C. Lintz, M. A. De Carvalho, and R. A. Franco, "Voids identification in rubberized mortar digital images using k-means and watershed algorithms," *Journal of Cleaner Production*, vol. 164, pp. 455–464, 2017.

[118] T. Gupta, S. Chaudhary, and R. K. Sharma, "Mechanical and durability properties of waste rubber fiber concrete with and without silica fume," *Journal of Cleaner Production*, vol. 112, pp. 702–711, 2016.

[119] G. Lazorenko, A. Kasprzhitskii, and E. H. Fini, "Polyethylene terephthalate (PET) waste plastic as natural aggregate replacement in geopolymer mortar production," *Journal of Cleaner Production*, vol. 375, p. 134083, 2022.

[120] M. Sifan, B. Nagaratnam, J. Thamboo, K. Poologanathan, and M. Corradi, "Development and prospectives of lightweight high strength concrete using lightweight aggregates," *Construction and Building Materials*, vol. 362, p. 129628, 2023.

[121] A. S. Ouda and A. M. Rashad, "An investigation on the performance of lightweight mortar-based geopolymer containing high-volume LECA aggregate against high temperatures," *Environmental Science and Pollution Research*, vol. 29, no. 18, pp. 26631–26647, 2022.

[122] F. Ameri, P. Shoaei, S. A. Zareei, and B. Behforouz, "Geopolymers vs. alkali-activated materials (AAMs): A comparative study on durability, microstructure, and resistance to elevated temperatures of lightweight mortars," *Construction and Building Materials*, vol. 222, pp. 49–63, 2019.

[123] Z. Hongen, J. Feng, W. Qingyuan, T. Ling, and S. Xiaoshuang, "Influence of cement on properties of Fly-Ash-Based concrete," *ACI Materials Journal*, vol. 114, no. 5, pp. 745–763, 2017.

[124] S. A. Bernal, J. L. Provis, V. Rose, and R. M. de Gutierrez, "Evolution of binder structure in sodium silicate-activated slag-metakaolin blends," *Cement and Concrete Composites*, vol. 33, no. 1, pp. 46–54, 2011.

[125] L. Xue, Z. Zhang, and H. Wang, "Hydration mechanisms and durability of hybrid alkaline cements (HACs): A review," *Construction and Building Materials*, vol. 266, p. 121039, 2021.

[126] D. González-Betancur, A. A. Hoyos-Montilla, J. I. Tobón, and B. García, "Effect of artificial lightweight aggregates on interfacial transition zone in concrete," in *Proceedings of the 75th RILEM Annual Week 2021*, (Cham), pp. 489–498, Springer International Publishing, 2023.

[127] B. Sun, G. Ye, and G. de Schutter, "A review: Reaction mechanism and strength of slag and fly ash-based alkali-activated materials," *Construction and Building Materials*, vol. 326, p. 126843, 2022.

[128] Z. Jiao, Y. Wang, W. Zheng, and W. Huang, "Effect of Dosage of Alkaline Activator on the Properties of Alkali-Activated Slag Pastes," *Advances in Materials Science and Engineering*, vol. 2018, p. 8407380, 2018.

[129] R. Snellings, A. Salze, and K. Scrivener, "Use of X-ray diffraction to quantify amorphous supplementary cementitious materials in anhydrous and hydrated blended cements," *Cement and Concrete Research*, vol. 64, pp. 89–98, 2014.

[130] M. Echeverri-Aguirre, J. Molina, A. A. Hoyos-Montilla, H. Carvajal, and J. Rudas, "Heat flow modelling of the alkaline activation of fly ash with sodium hydroxide in the presence of portlandite," *Construction and Building Materials*, vol. 357, p. 129248, 2022.

[131] Peter C. Hewlett, *LEA'S Chemistry of cement and Concrete*. Oxford: Elsevier Ltd, 4th ed., 1998.

[132] G. Bhagath Singh and K. V. Subramaniam, "Evaluation of sodium content and sodium hydroxide molarity on compressive strength of alkali activated low-calcium fly ash," *Cement and Concrete Composites*, vol. 81, pp. 122–132, 2017.

[133] H. Du, L. Yang, W. Gao, and J. Liu, "Effects of characteristics of fly ash on the properties of geopolymer," *Transactions of Tianjin University*, vol. 22, no. 3, pp. 261–267, 2016.

[134] S. Diamond, "On the glass present in low-calcium and in high-calcium flyashes," *Cement and Concrete Research*, vol. 13, no. 4, pp. 459–464, 1983.

[135] E. Diaz, E. Allouche, and S. Eklund, "Factors affecting the suitability of fly ash as source material for geopolymers," *Fuel*, vol. 89, no. 5, pp. 992–996, 2010.

[136] Y. P. Arias, "Incidencia de la temperatura ambiente en la formación de compuestos cementantes mediante la activación alcalina de cenizas de carbón," Master's thesis, Universidad Nacional de Colombia, 2013.

[137] K. Mohan and H. Taylor, "Analytical Electron Microscopy of Cement Pastes: IV, β-Dicalcium Silicate Pastes," *Journal of the American Ceramic Society*, vol. 64, no. 12, pp. 717–719, 1981.

[138] J.-I. Suh, D. Jeon, S. Yoon, J. E. Oh, and H.-G. Park, "Development of strong light-weight cementitious matrix for lightweight concrete simply by increasing a water-to-binder ratio in $Ca(OH)_2 - Na_2CO_3-$ activated fly ash system," *Construction and Building Materials*, vol. 152, pp. 444–455, 2017.

[139] W. S. Yum, Y. Jeong, S. Yoon, D. Jeon, Y. Jun, and J. E. Oh, "Effects of $CaCl_2$ on hydration and properties of lime(CaO)-activated slag/fly ash binder," *Cement and Concrete Composites*, vol. 84, pp. 111–123, 2017.

[140] Y. Guo, T. Zhang, W. Tian, J. Wei, and Q. Yu, "Physically and chemically bound chlorides in hydrated cement pastes: a comparison study of the effects of silica fume and metakaolin," *Journal of Materials Science*, vol. 54, no. 3, pp. 2152–2169, 2019.

[141] A. Novak, "Hydrogen bonding in solids correlation of spectroscopic and crystallographic data," in *Large Molecules*, (Berlin, Heidelberg), pp. 177–216, Springer Berlin Heidelberg, 1974.

[142] S. A. Yaseen, G. A. Yiseen, and Z. Li, "Elucidation of Calcite Structure of Calcium Carbonate Formation Based on Hydrated Cement Mixed with Graphene Oxide and Reduced Graphene Oxide," *ACS Omega*, vol. 4, pp. 10160–10170, jun 2019.

[143] P. Yu, R. J. Kirkpatrick, B. Poe, P. F. McMillan, and X. Cong, "Structure of Calcium Silicate Hydrate (C−S−H): Near−, Mid−, and Far-Infrared Spectroscopy," *Journal of the American Ceramic Society*, vol. 82, no. 3, pp. 742–748, 1999.

[144] A. Fernández-Jiménez and A. Palomo, "Mid-infrared spectroscopic studies of alkali-activated fly ash structure," *Microporous and Mesoporous Materials*, vol. 86, no. 1, pp. 207–214, 2005.